JOURNAL OF GEOPHYSICAL RESEARCH, VOL. 106, NO. C10, PAGES 22,355–22,372, OCTOBER 15, 2001

A quasi-one-dimensional coupled climate–carbon cycle model 2. The carbon cycle component

L. D. Danny Harvey

Department of Geography, University of Toronto, Toronto, Ontario, Canada

Abstract. A quasi-one-dimensional, coupled climate–carbon cycle model is presented which consists of two polar domains and one nonpolar domain. The model simulates the distribution of dissolved inorganic carbon (DIC), alkalinity, phosphate, dissolved oxygen, and temperature and contains a biological pump with production of organic tissue, calcite, and arogonite. Bottom water is conditioned in one polar domain through interaction with the atmosphere and convective mixing and is injected into the lower portion of the nonpolar domain. Intermediate water flows into the other polar domain and upwells. Successful simultaneous simulation of the observed distribution of all the tracers (including isotope ratios) requires (1) an upwelling velocity in the nonpolar domain that peaks around 2 m yr^{-1} at a depth of 1 km, with a gradual decrease above and below this depth; (2) effective vertical diffusion coefficients for temperature and other tracers that are different in the upper 0.5 km; and (3) a carbonate carbon to organic carbon production ratio of only 0.09. These requirements are consistent with physical considerations and/or observational evidence. In particular, observational data combined with a consideration of mixing along isopycnal surfaces and model results both indicate that the effective vertical diffusion coefficient in the upper ocean should be smallest for temperature and largest for oxygen, with the values for alkalinity and phosphate modestly smaller than for DIC. The model parameters obtained by tuning the model to preindustrial tracer distributions also provide the best (and generally excellent) fit to observed transient isotope changes. Interactions between alkalinity and DIC modulate the effect on steady state atmospheric pCO_2 of changes in the model parameters. However, the model uptake of anthropogenic CO_2 and the computed atmospheric CO_2 variation to year 2200 are remarkably insensitive to the choice of model mixing parameters, given that these are assumed to be constant during a given simulation. Finally, the sensitivity of the model atmospheric pCO_2 to changes in the temperature of warm ocean surface matches that obtained by three-dimensional ocean carbon cycle models.

1. Introduction

This is part 2 of a two-part series of papers that presents a quasi-one-dimensional, coupled climate-carbon cycle model. *Harvey and Huang* [this issue], herein after referred to as part 2, presented the model structure and the climate component of the model, and the difference between the climate component and the classical upwelling-diffusion (UD) climate model were documented. Here, the carbon cycle component of the model and its behavior are presented.

Very little work has been done in which the same ocean model is used to calculate the concurrent uptake of both heat and CO_2, given a scenario of anthropogenic CO_2 emissions. As discussed in part 1, the UD model has been used to examine the transient response of surface air temperature to imposed increases of atmospheric greenhouse gas (GHG) concentrations or to examine the role of the oceans in taking up anthropogenic CO_2. In work where the uptake of both heat and CO_2 have been computed using the one-dimensional (1-D) UD model [e.g., *Schimel et al.*, 1997], the same vertical diffusion coefficient (K_v) has been used for both heat and CO_2. As given by *Harvey and Huang* [this issue] and discussed more thoroughly here, the appropriate diffusion coefficient is decidedly different for heat and CO_2. Coupled atmosphere-ocean general circulation models (AOGCMs) have been used to examine the transient surface temperature response to imposed gradual increases in atmospheric CO_2, while the oceanic component of AOGCMs has been run as the oceanic component of the carbon cycle and used to compute the uptake of anthropogenic CO_2 with fixed circulation and temperature fields [*Maier-Reimer and Hasselmann*, 1987; *Sarmiento et al.*, 1992; *Taylor*, 1995]. They have also been used, as have the simpler 1-D models, to investigate the impact on atmospheric CO_2 concentration of imposed changes in the ocean circulation [*Bacastow and Maier-Reimer*, 1990]. A dynamical two-dimensional ocean model has also been used as part of a coupled atmosphere-ocean climate model [*Stocker et al.*, 1992] and to simulate the oceanic uptake of CO_2 with a fixed ocean circulation [*Stocker et al.*, 1994]. However, with the exception of *Joos et al.* [1999], no results have been published yet in which a coupled climate-carbon cycle model is driven by anthropogenic emissions of CO_2, with the same ocean model used to compute the uptake of both CO_2 and heat, and in which the subsequent atmospheric CO_2 and temperature changes are both able to respond to the computed variation in the oceanic uptake of CO_2 and heat.

Sarmiento and Le Quéré [1996] used a coupled atmosphere – ocean general circulation model, driven by the heating effect of

Paper number 2000JC000365.
0148-0227/01/2000JC000365$09.00

increasing atmospheric CO_2 concentration, to investigate the impact of ocean circulation changes on the rate of absorption of anthropogenic CO_2 by the oceans. The OGCM was used to compute the uptake of both heat and anthropogenic CO_2. However, in their experiments the CO_2 concentration scenario was fixed so that there was no feedback between changes in CO_2 uptake, the subsequent atmospheric CO_2 concentration, and subsequent temperature changes.

Maier-Reimer et al. [1996] avoided this shortcoming in a study in which an OGCM was driven by a prescribed pattern of surface temperature change. The surface temperature changes were scaled by the change in atmospheric CO_2 concentration, which depended on prescribed emissions and the model-computed uptake of CO_2 by the oceans. Thus the evolution of atmospheric CO_2 responded to changes in the computed uptake of CO_2 by the ocean, which varies as both the model ocean circulation and surface temperature change. However, in nature, changes in ocean circulation would lead to changes in the rate of uptake of heat by the oceans, which in turn would alter the rate of change of surface temperature. Such direct circulation feedbacks on temperature change can be dramatic, as discussed by *Harvey* [1994], but were omitted by the *Maier-Reimer et al.* [1996] study since the surface temperature boundary condition in their model was linked to atmospheric CO_2 concentration in a manner which was independent of whatever changes in ocean circulation (and other mixing processes) might occur. Thus coupled AOGCMs as well as 1-D models have yet to be used to compute the simultaneous uptake of both heat and CO_2 by the oceans in a fully consistent manner.

The purpose of this paper and of part 1 is to present a relatively simple coupled atmosphere-ocean climate-carbon cycle model that can be used to simulate the concurrent uptake of both heat and CO_2 by the oceans. The model can be used in the analysis of alternative greenhouse gas emission scenarios and in the study of the effect of hypothetical feedbacks between climate and the oceanic mixing parameters. As explained in part 1, the model to be presented here is not intended to predict changes in oceanic circulation. Rather, the present model is intended as a tool to diagnose the appropriate present-day mixing parameters (within observational constraints) and in analyzing the effect on the uptake of both heat and CO_2 of imposed feedbacks between climate and oceanic mixing.

Simple models can provide useful insights that aid in the interpretation and understanding of more complex models and have been widely used in the analysis of alternative scenarios of greenhouse gas emissions [*Harvey et al.*, 1997]. It turns out that the values of K_v, the upwelling velocity (w), and the biological pump strength that are deduced here are significantly different than generally used in simple models. Although these differences are not particularly important for the oceanic uptake of anthropogenic CO_2 in the absence of ocean circulation changes, they are important for the response of atmospheric CO_2 and temperature change when large changes in the ocean circulation occur (L.D.D. Harvey, manuscript in preparation, 2001). This provides an important justification for the development of the present model, and considerable effort is devoted to showing that the parameter values deduced for the present model are consistent with a wide range of observational constraints.

The remainder of this paper is organized as follows: section 2 describes the purely carbon cycle related features of the model. Section 3 presents the model simulation of preindustrial tracer fields, with particular emphasis on the alkalinity budget due to the absence of alkalinity as a variable in most previous 1-D models. Section 4 shows the sensitivity of the steady state simulation to changes in the key model parameters, with particular emphasis on the choice of K_v and of the upwelling velocity. Section 5 examines the base case transient isotope variations, their sensitivity to the same parameter changes as considered in section 4, and the sensitivity of the oceanic uptake of anthropogenic CO_2 to these parameter changes. Section 6 presents conclusions.

2. Model Description

The model structure, similarities with and differences from other models, and the framework and justification for the treatment of diffusion, convection, and upwelling, are all thoroughly explained in part 1. Readers not interested in the climate-related components and behavior of the present model should nevertheless read section 2 of part 1, particularly the "Model Overview." Here the broadest features of the model are recapitulated, further details concerning diffusion and convection (specific to carbon cycle variables) are discussed, and the formulation of the marine biosphere is presented.

As discussed in part 1, the model presented here contains atmospheric, oceanic, and terrestrial biosphere components. The terrestrial component consists of the six-box, globally aggregated terrestrial biosphere model of *Harvey* [1989]. The atmospheric component of the model, including the formulation of surface-air exchanges of sensible and latent heat, infrared radiation, and solar radiation, is that of *Harvey and Schneider* [1985]. The atmospheric and oceanic components have three domains: a nonpolar domain (covering 90% of the ocean surface area) and two polar domains (covering 5% each). A single atmospheric CO_2 concentration is computed and used for interaction with the three ocean surface boxes and with the terrestrial biosphere. The nonpolar atmospheric box interacts thermally with an atmosphere-land surface slab so as to obtain the effect of the small land thermal inertia on the transient temperature response, but this slab does not enter into the model in any other way. Bottom water is conditioned in one polar domain, while upwelling occurs in the other polar domain and in the nonpolar domain. Convective mixing occurs in both polar domains. The model allows for a variable ocean depth in the nonpolar domain based on observed global-mean ocean bathymetry. Seven tracer fields are simulated: temperature, three isotopes of dissolved inorganic carbon (DIC), total alkalinity (TALK), total dissolved phosphate (TPO_4) and dissolved oxygen.

2.1. Formulation of the Vertical Diffusion Coefficient

As discussed in part 1, the vertical diffusion coefficient used in the nonpolar domain for tracer X, K_X, is an effective coefficient that represents the net effect of mixing perpendicular to and along sloping isopycnal surfaces. It depends on the gradient on isopycnal surfaces of the tracer being diffused and therefore differs from tracer to tracer. Observational data were presented in part 1 indicating that K_X should be largest for dissolved oxygen, identical for all three isotopes of carbon, modestly smaller for TALK and TPO_4, and smallest of all for temperature. We introduced the parameterization,

$$K_X(z) = \begin{cases} K_n(z) & \text{temperature} \\ K_n(z) + K_{1X}(z) & \text{all other tracers} \end{cases}, \qquad (1)$$

where $K_{1X}(z)$ is the enhancement in K_X due to isopycnal mixing and $K_n(z)$ is the diapycnal contribution to K_X and depends on the

vertical stability. Since it is not possible to accurately compute $K_{1X}(z)$ from observed data, it shall be determined by tuning the model to give the best fit to observed tracer distributions, subject to the relative absolute values given above. The variation of K_{1X} with depth will depend on the variation in the along-isopycnal tracer gradients, the isopycnal slope, and of the along-isopycnal mixing coefficient (K_i) with depth. The latter in particular should decrease with increasing depth, since K_i depends on mixing by mesoscale eddies, whose strength one can reasonably expect to decrease with increasing depth. Thus we adopt the simple assumption that K_{1X} is largest at the surface and decreases linearly to zero at some specified depth, z_0.

2.2. Treatment of Convection

As discussed in part 1, convection is assumed to occur over a portion of the polar sea columns, with the fraction involved in convective mixing decreasing with depth. Convective mixing in nature gradually progresses to successively greater depths as the cooling season progresses, with continuous air-sea exchange of CO_2 and O_2 during this process. However, the model is integrated using a 1-year time step. Air-sea exchanges during convection are accounted for as follows: convective mixing is performed by first mixing the appropriate fraction of the first two model layers, adjusting the O_2 and DIC content of the top layer due to air-sea exchange of O_2 and CO_2, then mixing a smaller fraction of the first three layers, adjusting the O_2 and DIC content of the first layer, and so on until convection has extended to the bottom of the column. This procedure in effect divides each 1-year time step into N ministeps that are distributed over the portion of the year where convection occurs, where N is the number of model layers (30). On each successive ministep, convective mixing involves a smaller fraction of the grid boxes but extends to a greater depth. At the end of the time step, a single mean tracer value is computed for each layer. For O_2, we reduce the difference between the mixed layer O_2 concentration and the 3% supersaturation value by a fraction f_{O2} each time convection deepens by one layer. According to *Broecker and Peng* [1982, p. 123], the time constant τ_{O2} for O_2 to equilibrate with the atmosphere would be 25 days for a 67 m thick surface layer (as used here) and average oceanic wind conditions. Assuming that convection to the maximum depth occurs over a period of 180 days, the minitime step length is 6 days and $f_{O2}=1-e^{-6/\tau O2}=0.21$. If τ_{O2} is shorter for high-latitude fall and winter conditions, the appropriate value of f_{O2} would be larger. For CO_2, the air-sea flux assumed to occur each time that convection deepens by one layer is T_{conv}/N times that which would occur during 1 year, where T_{conv} corresponds to the fraction of year during which convection occurs. A value of 0.5 gives reasonable simulation results and is consistent with the value assumed in computing f_{O2}. Use of the convective scheme presented here, with air-sea gas exchange as mixing proceeds to greater depths, is particularly important to the successful simulation of the observed O_2 profile.

2.3. Ocean Biological Processes and Other Details

Biological production of organic carbon and of $CaCO_3$ is computed using procedures found in other models, except that (1) separate aragonite and calcite production is allowed and (2) the fraction of organic carbon buried that redissolves is specified to vary with depth based on observations. Full details are given in appendix A. Other technical details are given in appendices B and C.

3. Model Spin-up Using Base Case Parameter Values

3.1. Base Case Parameter Values and Simulated Tracer Fields

In this section the model spin-up state using the Base Case parameter values, which provide the best overall fit between the model and observations, is presented. Table 1 lists the data sources for the mean tracer profiles (used for the tuning of model parameters) and for time series data (used later for model validation). In addition to seeking a close fit to the observed vertical profiles of mean ocean temperature, DIC, TALK, dissolved O_2, TPO_4, $\delta^{13}C$, and $\Delta^{14}C$, we seek to match the following observations: (1) a preindustrial atmospheric CO_2 concentration of 278.0 ppmv; (2) a nonpolar mixed layer pCO_2 slightly in excess of the atmospheric value, so that there is a net eflux of CO_2 from the warm water surface box to the atmosphere; (3) downwelling and upwelling polar mixed layer pCO_2 values which are 20-40 μatm and 10-20 μatm, respectively, below the atmospheric value; (4) nonpolar, downwelling polar, and upwelling polar mixed layer values of DIC, TALK, TPO_4, $\delta^{13}C$, and $\Delta^{14}C$ as given in Table 2 (where data sources are also indicated); (5) a preindustrial atmospheric $\delta^{13}C$ of about -6.4‰, based on *Tans* [1981]; (6) a depth for the zero saturation point for calcite of 3200-3400 m, based on *Sundquist* [1990] and *Opdyke and Walker* [1992]; and (7) a rate of net burial of $CaCO_3$ of about 0.2 Gt C yr^{-1}, based on *Siegenthaler and Sarmiento* [1993]. The target range of 20-40 μatm for the air-sea pCO_2 difference in the Northern Hemisphere polar region is based on two sources. First, *Takahashi et al.* [1993] indicate that the summer mixed layer pCO_2 is 40-70 μatm below atmospheric pCO_2 over a broad region of the North Atlantic Ocean, with mean annual values roughly 20-30 μatm below the atmospheric value. Second, *Tans et al.* [1990] computed a mean annual difference in the Atlantic subarctic region of 37 ppmv. For the upwelling region, we use Southern Hemisphere polar values. According to *Tans et al.* [1990], the air-sea pCO_2 difference in Southern Hemisphere polar regions is about half that in Northern Hemisphere polar regions, and we aim for this ratio here.

The adjustable model parameters are A_0 (which determines the diapycnal diffusion coefficient, K_n), the K_{1X}, τ_p (see equation 7 of part 1), the vertical mass fluxes in the polar columns (which together determine the upwelling velocity, w), the air-sea exchange coefficient (K_{as}), and the biological parameters P_h, Pf_{CO3}, and f_{arog} (see appendix A). The other model parameters have been directly determined from observations. Of the adjustable model parameters, A_0, τ_p, and w are constrained to within a factor of 2 or better by direct observations. Given these constraints, we tuned the model parameters to fit the tracer observations listed above using the following procedure: First, values for A_0 and τ_p, and the variation of w in the upper kilometers, were determined by matching the model mean temperature profile to observations, as these are the only parameters that noticeably affect the mean temperature profile. Next, values of K_{as} were determined by requiring that the mixed layer $\Delta^{14}C$ fall within the ranges given above, as this parameter has the single largest influence on mixed layer $\Delta^{14}C$. The K_{as} values are also somewhat constrained by the need to have the right mixed layer-atmosphere pCO_2 differences. A further constraint on the polar K_{as} arises from the fact that the polar K_{as} value strongly influences atmospheric $\delta^{13}C$. An initial guess for $K_1(0)$ is obtained by requiring roughly the right ocean mean $\Delta^{14}C$ and suitable vertical gradients of DIC, TALK, and TPO_4 in the upper km of the

Table 1. Sources for Time Series and Vertically Distributed Data Used in this Paper

Input or Validation Data	Reference
Prescribed Input Data	
Ocean bathymetry	*Levitus* [1982]
Global Mean Vertical Profiles for Initialization and Validation of Ocean Spin–Up	
Temperature and dissolved oxygen	*Levitus* [1982]
Dissolved phosphate	*Levitus et al.* [1993]
DIC and total alkalinity	*Takahashi et al.* [1981, Fig. 4]
$\delta^{13}C$	estimated from *Kroopnick* [1985]
$\Delta^{14}C$	*Shaffer and Sarmiento* [1995][a]
Time Series Input Data	
Atmospheric CO_2 variation, 1765-1997	*Keeling and Whorf* [1998]
Fossil fuel CO_2 emissions, 1765-1995	*Marland et al.* [1998]
Fossil fuel $\delta^{13}C$, 1850-1991	*Tans* [1981] for 1850-1950; *Andres et al.* [2000] for 1950-1991
Time Series of nuclear bomb test TNT	*Hesshaimer et al.* [1994]
Time Series for Validation of Model Transient Response	
Atmospheric $\delta^{13}C$ variation,	*Jain et al.* [1995]
Tropospheric $\Delta^{14}C$ variation, 1840-1990	*Stuiver and Quay* [1981, Figure 2] for 1840-1954; *Broecker et al.* [1995, Figure 17] for 1955-1990
Mixed layer $\Delta^{14}C$ variation, 1765-1980	Atlantic coral data, *Druffel and Suess* [1983, Figure 4]
Relative variation of Ocean bomb ^{14}C inventory, 1956-1990	*Broecker et al.* [1995, Table 3]
Global mean ocean vertical profile of bomb ^{14}C on Jan. 1, 1975	*Siegenthaler and Joos* [1992]
Ocean bomb ^{14}C inventory on Jan. 1, 1975	*Broecker et al.* [1995]

[a] Extrapolated from the 3-4 km depth to a depth of 6 km.

ocean. The biological parameters P_h and Pf_{CO3} also have a strong influence on the DIC and TALK profiles (and hence on the lysocline depth), while Pf_{CO3}, f_{arog} have a strong influence on the net $CaCO_3$ burial rate; these parameters are adjusted as required, with particular attention to the resultant mixed layer values of DIC and TALK. The plume detrainment profile, and the absolute values of K_n and w, have a particularly strong influence on the DIC, TALK, $\Delta^{14}C$ and O_2 profiles in the lower 2 km of the ocean (if K_n is too small or the detrainment too concentrated, the deep ocean gradients are too strong).

Table 3 lists the Base Case model parameter values, obtained as a result of the tuning exercise described above. The relative $K_I(0)$ values required for different tracers agree with the expectations based on the analysis of observed data presented in part 1; in particular, a substantially larger $K_I(0)$ is required for O_2 than for DIC, while best results are obtained when $K_I(0)$ for TALK and TPO_4 is ~15% less than for DIC. $K_I(z)$ is required to decrease to zero at a depth (z_0) of about 500 m, since use of a larger z_0 causes the vertical tracer gradients to be too weak in the upper ocean.

Table 2. Comparison of Tracer Concentrations in the Nonpolar and Polar Mixed Layer as Simulated by the Present Model Base Case and as Estimated for Preindustrial Conditions ($\Delta^{14}C$) or as Observed at Present (all other variables) [a]

Tracer	Model			Observed or Estimated		
	Nonpolar	DPD	UPD	Nonpolar	DPD	UPD
$(pCO_2)_a$-$(pCO_2)_{ML}$ (ppmv)[b]	-2.7	36.4	15.1	< 0	20-40	10-20
DIC (μmole kg^{-1})[c]	1973	2134	2194	2010±25[g]	1980	2180
TALK (μequiv kg^{-1})[c]	2309	2334	2386	2310±5	2290	2350
TPO_4 (μmole kg^{-1})[d]	0.53	0.93	1.07	0.44	0.63	1.30
$\delta^{13}C$ (‰)[e]	2.20	2.22	2.81	≈1.6[h]	> 1.6[h]	2.0-2.2[h]
$\Delta^{14}C$ (‰)[f]	-50	-86	-108	-40 to -60	-50 to –70	-80 to -120

[a] DPD, downwelling polar doman; UPD, upwelling polar domain.
[b] See text for sources of observed data.
[c] Observed data are from *Takahashi et al.* [1980].
[d] Observed data are from *Levitus et al.* [1993].
[e] Observed data are estimated from *Bacastow and Maier-Reimer* [1990, Figure 26].
[f] Observed data are from *Broecker et al.* [1985, Figures A1, A2, A6].
[g] Should be reduced by ≈ 50 μmole kg^{-1} for comparison with model results.
[h] Should be increased by ≈ 0.5% for comparison with model results.

Table 3. Base Case Parameter Values Adopted Here for the Non-polar and Polar Domains [a]

	Nonpolar	Polar
Parameter		
Maximum depth, m	6000	6000
Fractional area	0.90	0.10
Parameter in K_n parameterization, A_0, $m^2\ s^{-2}$	1.4×10^{-7}	---
$K_1(0)$ (DIC)	1.75 $cm^2\ s^{-1}$	---
$K_1(0)$ (TALK,TPO_4)	1.55 $cm^2\ s^{-1}$	---
$K_1(0)$ (O_2)	2.75 $cm^2\ s^{-1}$	---
Upwelling velocity, w, m yr^{-1} [b]	2.1 peak	---
Lateral mixing parameter, α, yr^{-1}	0.015 to 0.0001	
Air-sea exchange, K_{as}, mole $m^{-2}\ yr^{-1}\ \mu atm^{-1}$	0.07	0.07
Convective mixing parameters		
f_T	---	1.00
f_B	---	0.01
τ_{conv}, m	---	400
f_{O2}	---	0.25
f_{CO2}	---	0.50
Biological parameters		
L_{fac}	0.9	0.8
P_h, μmole kg^{-1}	1.45	1.45
Pf_{CO3}	0.129	0.129
f_{arog}	0.50	0.50
z_{POC}, m	400	400
r_{POC}	0.07	0.07
Sedimentation parameters		
Sf_{CO3}	0.93	0.93

[a] Dashed entries indicate that the parameter is not applicable to the domain in question.

[b] Upwelling value is averaged over the nonpolar and upwelling polar domains.

Figure 1 shows the variation in the total diffusion coefficient for the various tracers. Like *Siegenthaler and Joos* [1992], we find that a K_X for DIC (K_C) that strongly decreases with depth in the upper ocean is essential for the simultaneous simulation of preindustrial and bomb ^{14}C (the latter is discussed in section 5). The parameterization of the diapycnal component of K_C in terms of vertical stability does not reverse the K_C gradient in the upper ocean but gives the increase in K_C with an increasing depth in the deeper ocean that is required in order to get reasonable deep ocean tracer profiles. At the same time, the variation of K_T below the 1000 m depth has negligible effect on the temperature profile (because $\partial T/\partial z \approx 0$ below 1000 m).

We have chosen K_{as}=0.07 moles $m^{-2}\ yr^{-1}$ ppmv^{-1} in all three domains. *Sarmiento et al.* [1992, Figure 2) deduced K_{as} values over the ice-free ocean of ~0.05, 0.085, and 0.10 moles $m^{-2}\ yr^{-1}$ ppmv^{-1} at low latitudes, at 50°N, and at 50°S, respectively. Accounting for partial ice cover would greatly reduce these spatial differences. The required natural ^{14}C production rate is 3.0 x 10^{26} atoms yr^{-1}, which is somewhat more than the value of 2.3 x 10^{26} atoms yr^{-1} used by *Hesshaimer et al.* [1994].

Figure 2 compares the model profiles of DIC, TALK, TPO_4, O_2, $\delta^{13}C$, and $\Delta^{14}C$ with observations. The upper part of the observed DIC and $\delta^{13}C$ profiles includes an anthropogenic signal, which should be subtracted before comparison with the model simulation. The surface DIC should be reduced by ~ .5% (or 50 μmole kg^{-1}) and the surface $\delta^{13}C$ increased by ~0.5%. If these adjustments decay to zero at the 1 km depth, the apparent model error in the upper 1 km is largely eliminated. As shown in part 1, the temperature profile also compares well with observations.

The most significant remaining error concerns the O_2 concentration, which is too small at all depths below ~500 m. This may suggest that the biological pump is too strong or that too much remineralization of organic carbon falling onto the sea floor occurs. However, the fraction that is remineralized within the sediment column is based on observations. The pump strength for the base case is 11.1 Gt C yr^{-1}, which falls near the middle of the estimated observational range of 4-20 Gt C yr^{-1} given by *Siegenthaler and Sarmiento* [1993]. However, forcing the biological pump to be weak enough to eliminate the error in the O_2 minima seriously degrades the otherwise excellent TPO_4 profile. *Shaffer* [1996] found that he could obtain a near-perfect fit to the observed O_2 profile only if his diffusion coefficient (assumed to be the same for all tracers) is comparatively small (0.32 $cm^2\ s^{-1}$), so that the biological pump is small (4.6 Gt C yr^{-1}). However, *Emerson et al.* [1997] present data indicating that the biological pump in the subtropical oceans alone is 5-6 Gt C yr^{-1} and cite recent model-derived estimates for the global biological pump of 10-11 Gt C yr^{-1}.

The O_2 error can be largely eliminated if we set f_{O2}=0.5 rather than 0.25, to allow for greater air-sea exchange of O_2 in high latitudes during fall and winter than in the global mean. The result is shown as case "2 x Base f_{O2}" in Figure 2d. It is important to be able to demonstrate a close fit to the observed ocean O_2 profile using plausible assumptions for total remineralization and air-sea exchange, not because these parameters have any effect on the model dynamics, but because failure to obtain a reasonable O_2 profile would imply an error in the biological pump strength and/or in K or w. This would have an effect on the model dynamics if w changes as part of a climate-ocean circulation feedback (L.D.D. Harvey, manuscript in preparation, 2001).

The model simulates an atmospheric $\delta^{13}C$ of -6.48%, a $CaCO_3$ net burial rate of 0.22 Gt C yr^{-1}, and a depth at which the water becomes unsaturated with respect to calcite of 3784 m. The first two results compare well with observational estimates, but the calcite saturation horizon is 300-500 m too deep. Table 2 compares mixed layer tracer concentrations with observations or other estimates of the preindustrial values and indicates fairly good overall agreement.

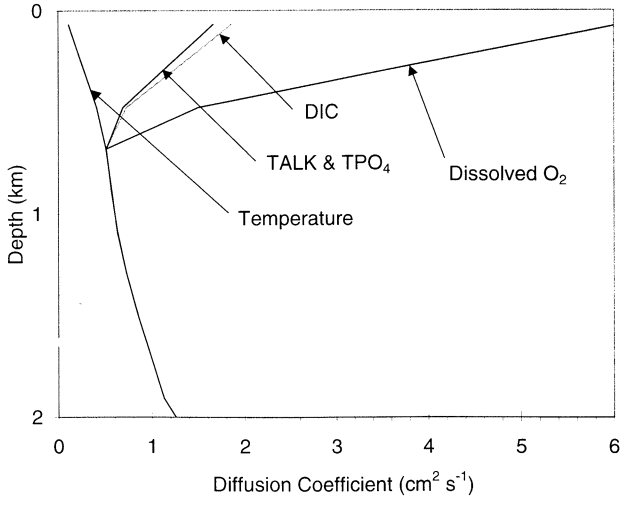

Figure 1. Comparison of the effective diffusion coefficient for various tracers in the upper 2 km of the ocean.

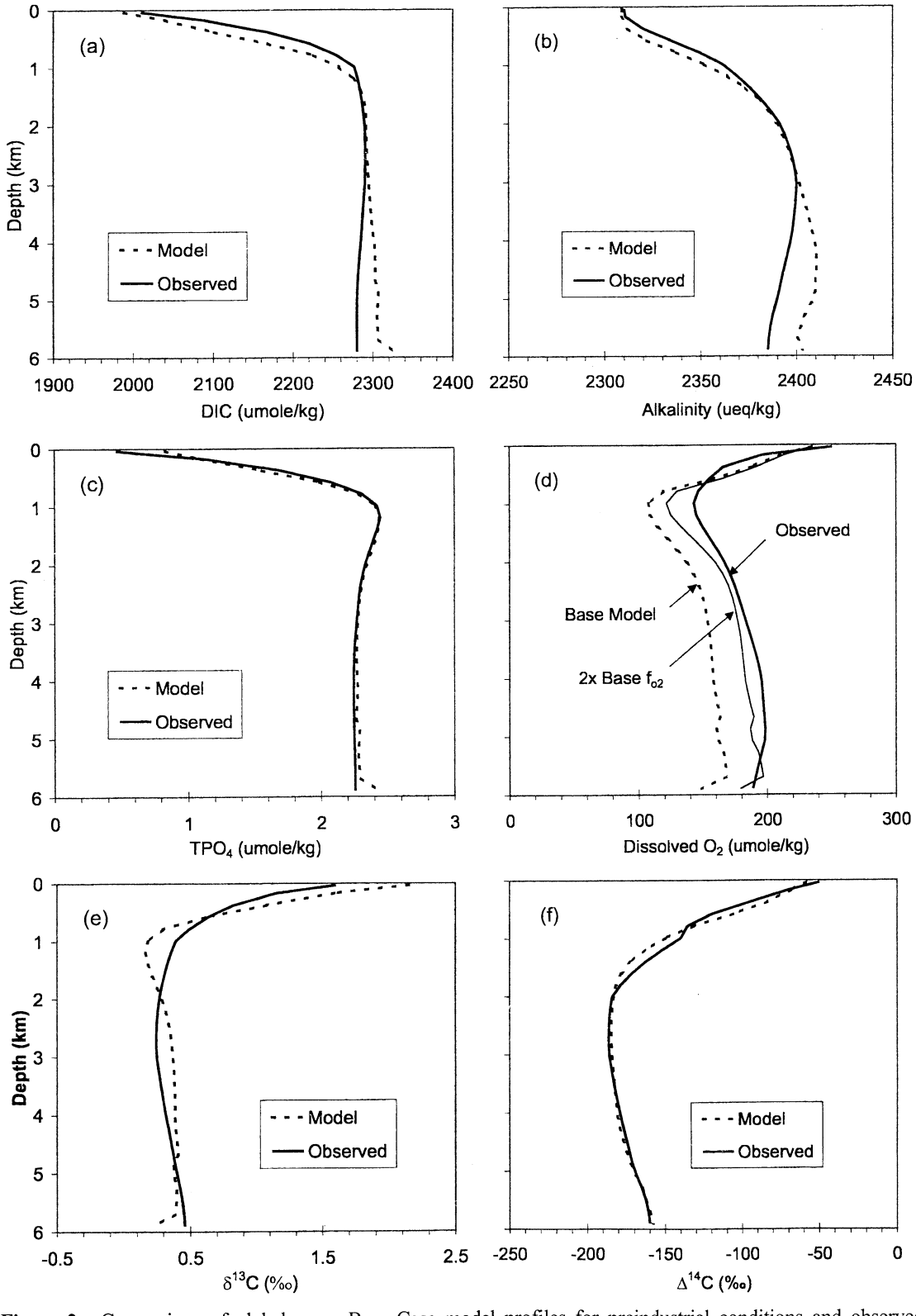

Figure 2. Comparison of global mean Base Case model profiles for preindustrial conditions and observed profiles for (a) DIC, (b) TALK, (c) TPO4, (d) dissolved O_2 , (e) $\delta^{13}C$, and (f) $\Delta^{14}C$. Case labeled "2 x Base f_{O2}" in Figure 2d is explained in the text. Observational data sources are listed in Table 1. All the observed profiles pertain to the mid – 1970s, except for $\Delta^{14}C$, which is the estimated preindustrial profile. As discussed in the text, the observed values for DIC and $\delta^{13}C$ in the upper ocean need to be adjusted for proper comparison with the model results.

Table 4. Mixed Layer Budgets for Carbon, Phosphorous, and Alkalinity for the Base Case Spin-up

	C Flux, Gt yr^{-1}			P Flux, Gt yr^{-1}	TALK Flux, Meq yr^{-1}		
	Warm	Polar	Total		Warm	Polar	Total
Riverine and/or volcanic input			0.57	0.0078	28.37	1.39	31.76
Soft tissue pump	7.41	2.93	10.34		-89.77	-35.46	-125.22
$CaCO_3$ pump	0.67	0.07	0.74		111.52	12.43	123.95
Total Bio-pump	8.08	3.00	11.08	0.2279	21.76	-23.09	-1.27
Advection			0.07	-0.0019			2.13
Convection		-2.60	-2.60	-0.0659		19.56	19.56
Diffusion	-8.11		-8.11	-0.1548	9.35		9.35
Shallow burial			0.13	0.0025			2.00
Net to deep ocean			0.44	0.0053			29.76

[a] Positive terms are downward fluxes.

3.2. Mixed Layer Carbon, Alkalinity, and Phosphate Budgets

An understanding of the dominant terms in the mixed layer budgets for DIC, TALK, and TPO_4 can be helpful in understanding the response of mixed layer pCO_2 to possible changes in ocean circulation. These budgets are presented in Table 4. In the case of DIC and TPO_4, the dominant balance is between a downward flux due to the biological pump and an upward flux due to diffusion. The convective fluxes are also upward and about one third as large as the diffusive flux, while the advective fluxes are negligible owing to the fact that the DIC and TPO_4 concentrations in sinking polar water are almost the same as the concentrations in water that upwells into the nonpolar mixed layer. In both cases there is a small net flux into the deep ocean that equals the riverine (in the case of TPO_4) or riverine plus volcanic (in the case of DIC) inputs minus net burial within the mixed layer.

As seen from Table 4, the ratio of carbonate-to-organic tissue carbon production ($CaCO_3$:C_{org}) is only 0.072, which is much less than the value of 0.25 that *Broecker and Peng* [1982] estimated using a two-box model. Most of the $CaCO_3$ production occurs in the nonpolar box due to the temperature-dependence of $CaCO_3$ production. Increasing the $CaCO_3$:C_{org} ratio in the present model results in too small a surface alkalinity, too deep a lysocline, and too large a $CaCO_3$ burial rate unless C_{org} is reduced, in which case other significant errors arise. *Yamanaka and Tajika* [1996] also found it necessary to assume a small $CaCO_3$:C_{org} ratio (between 0.08-0.10), using an OGCM, and cite observational evidence supporting a ratio this low.

The biota are normally thought of as causing a net downward alkalinity transfer, in association with falling $CaCO_3$ particles, as well as a downward carbon transfer. A downward alkalinity transfer would tend to reduce the surface alkalinity and thereby increase the surface pCO_2. Here, however, the net biological alkalinity transfer is close to zero because the $CaCO_3$:C_{org} production ratio (1:14.0) is about half the N:C ratio in organic matter (1:7.3). The net alkalinity flux is downward in the nonpolar region and upward in the polar regions because there is essentially no $CaCO_3$ production in the polar region. This is the reason why the surface alkalinity is higher in the polar regions than in the nonpolar region. It also implies that as the soft tissue pump changes strength, opposite effects on the net alkalinity pump will occur in polar and nonpolar regions. As a result of higher polar alkalinity, the polar pCO_2 is smaller than it would be for a given DIC, so that a larger DIC of sinking water is possible; this in turn influences the net vertical carbon flux caused by thermohaline overturning (the advective flux).

The TALK budget differs from the DIC and TPO_4 budgets in several important ways: (1) the advective flux is nonnegligible, (2) the biological flux is small (as noted above); and (3) the net flux to the deep ocean is the result of large fluxes generally in the same direction, rather than being the small residual of large fluxes in opposing directions. Insight into the last point is obtained by examining the component alkalinity flows, which are illustrated in more detail in Figure 3. The downward alkalinity flux associated with $CaCO_3$ particles is deposited deep in the ocean, where $CaCO_3$ dissolution occurs, whereas the upward flux associated with the consumption of NO_3^- in the mixed layer originates from the top few hundred meters of the ocean, where most organic matter decay occurs. This spatial mismatch in the source/sink regions for Ca^{2+} and NO_3^- creates a slight subsurface alkalinity minima which causes the diffusive flux at the base of the mixed layer to be downward. The convective flux is downward because the biological flux is strongly upward in the polar regions, creating a surface alkalinity maxima. This high polar surface alkalinity, combined with the aforementioned alkalinity minima in upwelling water below the nonpolar mixed layer also explains the strong downward advective alkalinity flux.

4. Sensitivity of the Spin-up State to Alternative Parameter Values

In this section we examine the sensitivity of the spin-up state to alternative choices of those model parameters having the greatest effect on the model solution. Table 5 gives the atmospheric pCO_2, the difference between atmospheric and downwelling polar mixed layer pCO_2, the DIC, and TALK concentrations in the nonpolar surface box, the biological pump strength, the $CaCO_3$ burial rate, and the depth of the zero-saturation level for calcite for the Base Case and for selected sensitivity tests. Figure 4 shows the impact on the $\Delta^{14}C$ profile when K_1, A_0, w, and K_{as} are varied, while Figure 5 shows the impact on the DIC profile when K_1, A_0, and w are varied (the changes in DIC are representative of the change in TALK and TPO_4 for these parameter changes, while changing K_{as} has a noticeable effect only on the $\Delta^{14}C$ profile). Doubling the upwelling velocity

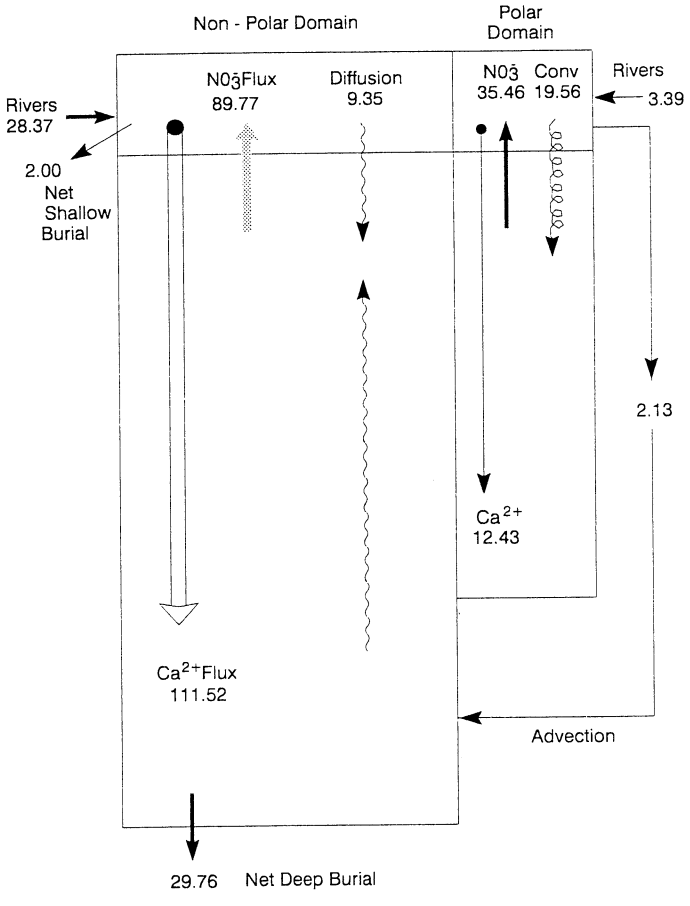

Figure 3. Alkalinity flows (in millions of equivalents per year) for the Base Case model spin-up.

at all depths or doubling the stability-dependent part of K by doubling A_0 increases mixed layer DIC and TALK, strengthens the biological pump, deepens the zero-saturation level, and increases the $CaCO_3$ burial rate. Increasing surface DIC and TALK have opposing effects on pCO_2, but the DIC effect dominates, so that pCO_2 increases as either A_0 or w are increased. These changes can be offset by altering P_h and Pf_{CO3} but the mean ocean $\Delta^{14}C$ (-120%) are too large when A_0 and w are doubled. The mean ocean $\Delta^{14}C$ can be brought in line with observations (-160%) by reducing K_{as}, but then the surface $\Delta^{14}C$ values are too small. Furthermore, deep ocean dissolved oxygen (not shown) is far too high using doubled A_0 and w. Thus we cannot simultaneously simulate all the observed tracer profiles if we use a peak upwelling velocity comparable to the often-used value of 4 m yr^{-1} suggested by *Hoffert et al.* [1980]. Furthermore, we cannot get a good simulation of all the tracer profiles if w is not assumed to gradually increase with increasing depth in the upper ocean and gradually decrease in the lower ocean.

Similarly, any substantial change in the values of $K_1(0)$ from

Table 5. Impact on Atmospheric pCO_2, the Difference Between the Atmospheric pCO_2 and the Polar Mixed Layer pCO_2, and Other Model Results, when the Upwelling Velocity (w), Diffusion Coefficient Parameter (A_0), $CaCO_3$ Production Parameter (Pf_{CO3}), or Scale Depth for Settling Organic Debris (z_{POC}) are Doubled, the Arogonite Fraction (f_{arog}) Set to Zero, or the C:P Redfield Ratio (R_{CP}) Increased by 20%

Parameter Change	Atm PCO_2, µatm	Atm-DPD pCO_2	Atm-UPD pCO_2	Warm ML DIC, µmole kg^{-1}	Warm ML TALK, µequiv kg^{-1}	Bio Pump, Gt C y^{-1}	$CaCO_3$ Burial, Gt C y^{-1}	Calcite Saturation Depth, m
Base Case	278	37	15	1967	2304	11.1	0.22	3784
2 x w	288	47	19	1990	2323	13.1	0.33	4274
2 x A_0	288	38	16	1996	2320	12.5	0.26	3792
2 x w, A_0	294	48	19	2007	2332	14.2	0.36	4197
2 x Pf_{CO3}	304	40	20	1924	2226	11.9	0.59	4533
f_{arog}=0.0	274	37	15	1977	2318	11.1	0.32	3756
2 x z_{POC}	256	36	12	1970	2327	8.1	0.08	2791
1.2 x R_{CP}	246	36	15	1925	2282	13.3	0.26	3774

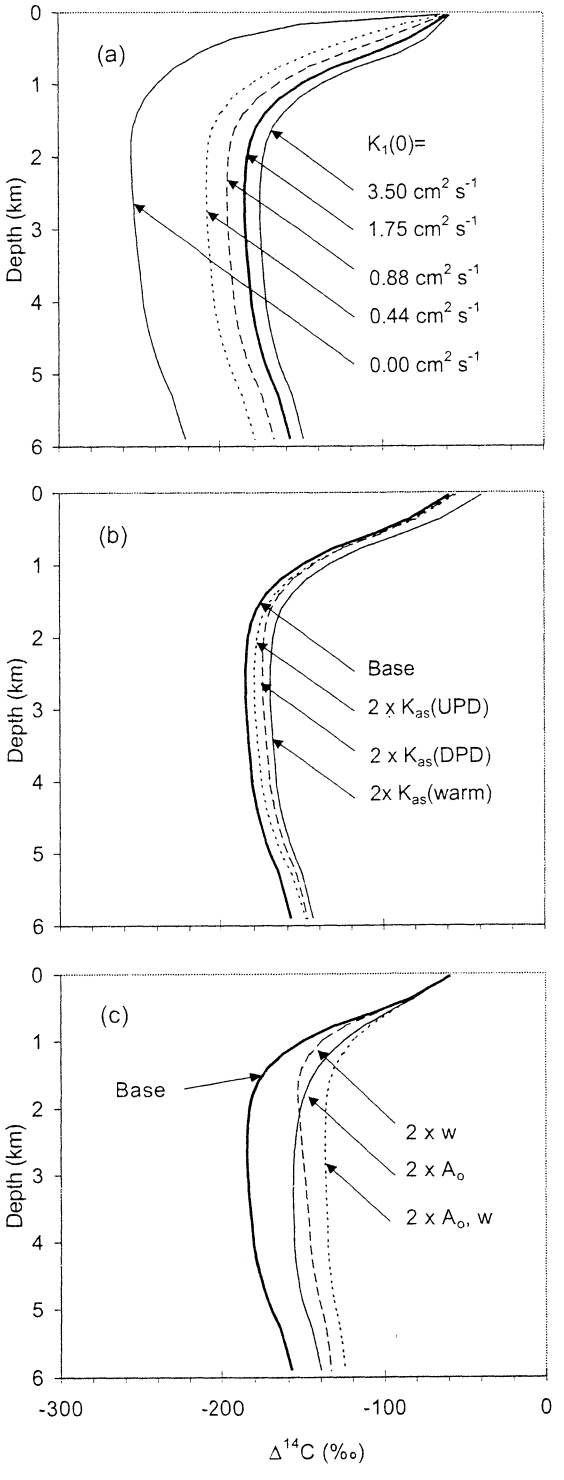

Figure 4. Comparison of the spin-up profile of $\Delta^{14}C$ as (a) the value of the supplemental diffusion coefficient at the base of the mixed layer, $K_1(0)$, is varied, (b) as the air-sea exchange coefficient K_{as} is varied, and (c) as the stability-dependent part of the vertical diffusion coefficients and the upwelling velocity are uniformly changed.

our Base Case values creates substantial errors in the $\Delta^{14}C$ and DIC profiles (shown in Figures 4a and 5a), as well as in the TALK, TPO_4, and $\delta^{13}C$ profiles (not shown). Conversely, setting f_{CO2}=0.0 (no air-sea CO_2 exchange during convective mixing) has a negligible effect on the simulation.

When the $CaCO_3$:C_{org} ratio is increased from 0.07 to 0.14 (by doubling Pf_{CO3}), the surface alkalinity decreases as expected. Decreasing TALK for a given DIC raises the pCO_2, causing an outgassing of CO_2 and a decrease in DIC about half as large as the initial decrease in TALK (i.e., a DIC decrease of 43 μmole kg^{-1}, compared to a TALK decrease of 78 μequiv kg^{-1}). The resultant surface TALK is far too low, while the calcite saturation depth and total $CaCO_3$ burial rate are too large. This reiterates our earlier point that we require a much smaller $CaCO_3$:C_{org} ratio than commonly accepted. Assuming all of the $CaCO_3$ production to be calcite, rather than 50% arogonite, has a modest effect on all the model variables except the $CaCO_3$ burial rate, which increases by about half (Table 5). As with changes in the $CaCO_3$:C_{org} production ratio, the effect of a change in the aragonite:calcite production ratio on mixed layer DIC is about half as large as the effect on mixed layer TALK.

Increasing the scale depth for the decomposition of falling organic matter, z_{POC}, weakens the biological pump because nutrients are released at greater depths in the ocean. This allows both DIC and TALK to increase, but the tendency for surface DIC to increase is partly offset by the fact that there is less upward diffusion of DIC due to the greater depth at which organic carbon is released. As a result, the increase in mixed layer

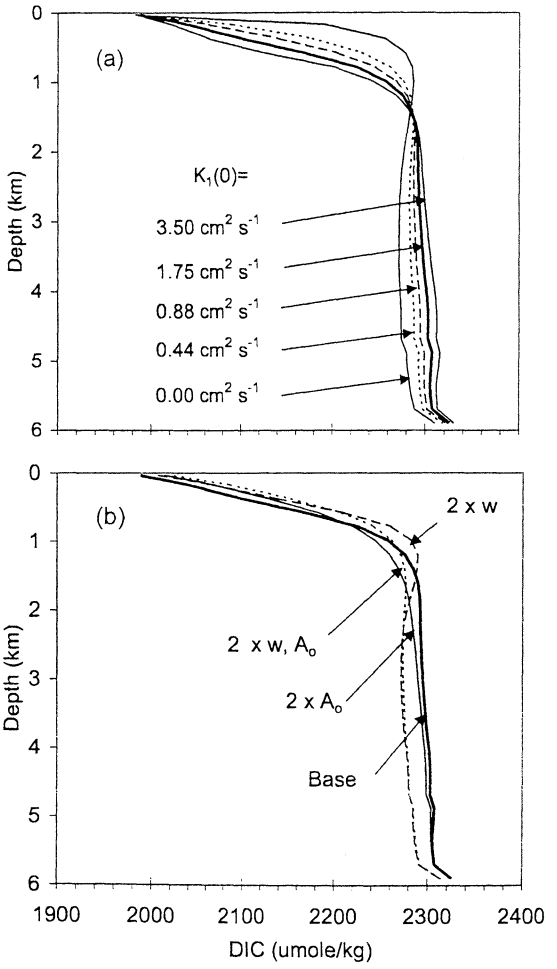

Figure 5. Comparison of the spin-up profile of DIC as (a) the value of the supplemental diffusion coefficient at the base of the mixed layer, $K_1(0)$, is varied and (b) as the stability-dependent part of the vertical diffusion coefficients and the upwelling velocity are uniformly changed.

TALK is ~8 times larger than the increase in mixed layer DIC, and the increase in TALK dominates the pCO_2 response, which shows a sharp decrease in spite of the weaker biological pump. This example illustrates the importance of feedbacks involving TALK, since the initial perturbation has negligible direct effect on TALK, yet the surface TALK response dominates the atmospheric pCO_2 response.

A 20% increase in the C:P Redfield ratio increases the biological pump strength by 20% and reduces atmospheric pCO_2 by ~10%. In the nonpolar mixed layer, DIC decreases by 2.1%, TALK decreases by 1.2% (due to the fact that $CaCO_3$ production increases with increased organic carbon production), and pCO_2 decreases by 11.5%. The decrease in TALK greatly diminishes the impact on pCO_2 of the decrease in DIC since, given a buffer factor of 9.2, the DIC decrease would decrease pCO_2 by ~19% with constant TALK, almost twice that observed. This is another illustration of the importance of interactions involving alkalinity for the CO_2 response to changes in model parameters.

5. Transient Response of Model Isotopes and of Atmospheric CO_2

Jain et al. [1995, 1996] showed that their model is able to accurately simulate the preindustrial global mean oceanic profiles of DIC and $\Delta^{14}C$, as well as the observed historical variation of atmospheric and oceanic isotope ratios. However, they presented results for only one set of model parameters, so it is not clear from their work how sensitive the transient isotope distributions are to changes in model parameters, and hence, the extent to which the isotope distributions can be used to constrain the model parameters. As shown in the preceding section, the steady state oceanic $\Delta^{14}C$ profile (and, to a lessor extent, the $\delta^{13}C$ profile) is very sensitive to decreases in $K_1(0)$ from our base case value, and is moderately sensitive to changes in K_n below the 1 km depth, in the upwelling velocity, and in K_{as}. In this section we first compare the Base Case model simulation of transient carbon isotope variations with observations, then illustrate the sensitivity of the transient isotopic response to changes in selected model parameters, and, finally, compare this sensitivity with the sensitivity of the oceanic uptake of anthropogenic CO_2 to the same parameter changes.

5.1. Base Case Response of Isotopes

Figure 6 compares the Base Case model and observations for (a) the variation of atmospheric $\delta^{13}C$ for 1800-1990, (b) the variation of atmospheric $\Delta^{14}C$ for 1800-1950, (c) the variation of tropospheric $\Delta^{14}C$ from 1950-1990, and (d) the change in $\Delta^{14}C$ as a function of depth at the end of 1974 due to the penetration of bomb ^{14}C. A perfect fit to the atmospheric CO_2 variation is achieved by running the model in inverse mode up to 1990 [see *Wigley*, 1991] and determining the required land use emissions. It is also possible to achieve a close fit to the ob-

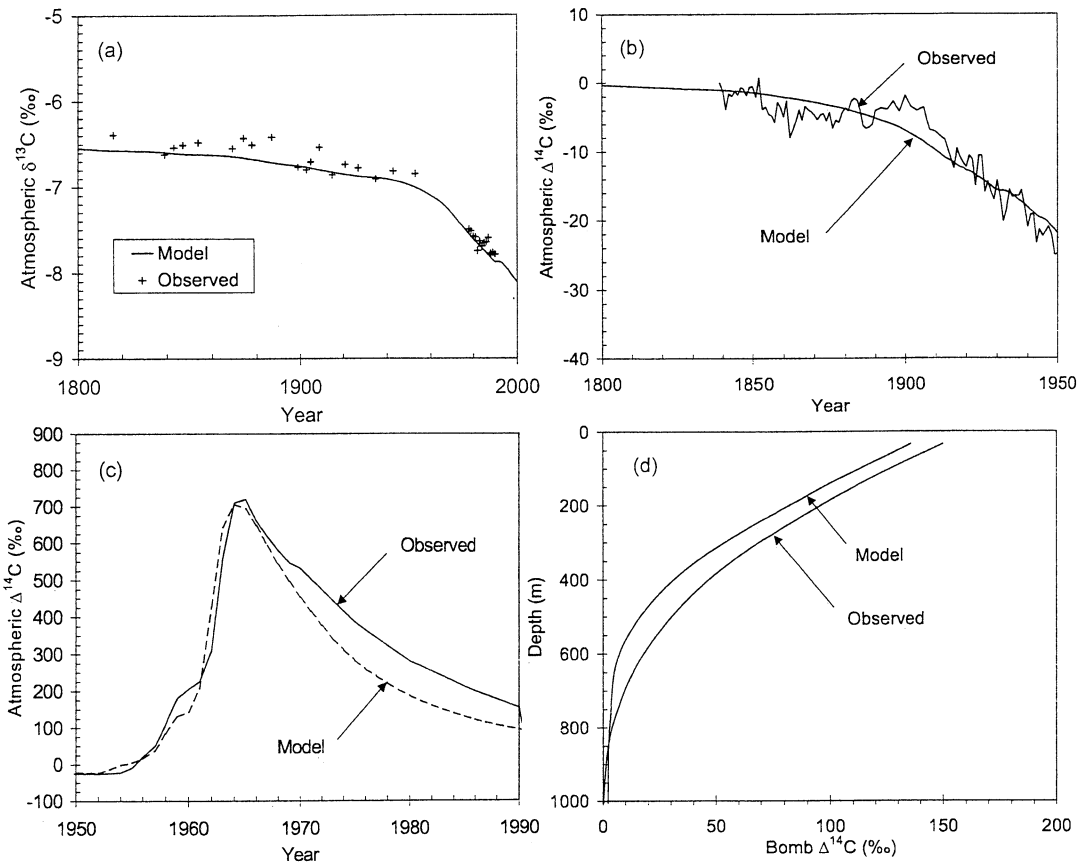

Figure 6. Comparison of Base Case model results and observations for (a) the variation of atmospheric $\delta^{13}C$, (b) the variation of atmospheric $\Delta^{14}C$ prior to the period of nuclear bomb testing, (c) the variation of tropospheric $\Delta^{14}C$ from 1950-1990, and (d) the global mean profile of bomb ^{14}C on January 1, 1975. Observational data sources are listed in Table 1.

served global mean temperature variation by choosing the climate model temperature sensitivity to a CO_2 doubling and the cooling effect of aerosol emissions within the range of the estimated uncertainty (see L.D.D. Harvey and R. Kaufmann, manuscript in preparation, 2000). The ability to simulate the observed atmospheric CO_2 and global mean temperature variation therefore does not serve as a constraint on the model mixing parameters, so these results are not shown here.

The change in atmospheric $\delta^{13}C$ for 1800-1990 is due largely to the dilution of atmospheric CO_2 with isotopically light fossil fuel carbon and is in excellent agreement with the observations (Figure 6a). The decrease in atmospheric $\Delta^{14}C$ up to 1950 is due to dilution of atmospheric CO_2 with ^{14}C-free fossil fuels (the Suess effect). The model-simulated decrease from 1860 to 1950 is 19.7% (Figure 6b), compared to an observed decrease between the 1855-1864 decade and the years 1949-1951 of 20.0±1.2% given by *Stuiver and Quay* [1981]. However, the observed change contains contributions due to variations in the Earth's geomagnetic field and in solar variability, which *Stuiver and Quay* [1981] estimate to be 2.1% and -4.8%, respectively. These estimates are themselves dependent on model calculations but imply that the component of the observed $\Delta^{14}C$ variation due to fossil fuel combustion is -17.3±1.2%. In this case, the model decrease in $\Delta^{14}C$ is slightly too large.

Atmospheric testing of nuclear bombs occurred during the period 1952-1981 and injected large amounts of ^{14}C directly into the stratosphere. This led to a sharp spike in atmospheric $\Delta^{14}C$, which subsequently declined owing to absorption of ^{14}C by the oceans and terrestrial biosphere. In order to compare the model response to bomb ^{14}C injections with observations, we divided our atmospheric box into a separate stratosphere and troposphere, with the stratosphere containing 20% of the atmospheric mass. We have chosen a turnover time of stratospheric air with respect to the troposphere of 3 years, which is the middle of the observationally based range of 3±1 given by *Broecker and Peng* [1994] for the exchange of midstratospheric air with the troposphere. The ^{14}C production from nuclear bomb testing is estimated to lie between 1-2 x 10^{26} atoms per Mt TNT equivalent and, for lack of adequate data, is generally assumed to have been constant [*Hesshaimer et al.*, 1994]. We obtain the best overall results using a ^{14}C yield of 1.0 x 10^{26} atoms per Mt-TNT.

The decrease in tropospheric $\Delta^{14}C$ from its peak value around 1965 is initially too fast (Figure 6c), while the vertical profile of the change in $\Delta^{14}C$ at the end of 1974 is very close to the observational estimate (Figure 6d). The error in the tropospheric $\Delta^{14}C$ obtained here is in the same direction but much smaller than the error obtained by *Hesshaimer et al.* [1994]. They interpreted their error as an indication that the uptake of bomb ^{14}C in their ocean model and, by extension, the uptake of anthropogenic CO_2, was 25% too large. Since the model uptake was calibrated to match the estimated observed uptake by 1975, they suggested that the observational estimate of bomb ^{14}C uptake by the oceans, and previous estimates of anthropogenic CO_2 uptake, are 25% too large. The error in the tropospheric $\Delta^{14}C$ shown in Figure 6c is extensively analyzed by L.D.D. Harvey (manuscript in preparation, 2001), where quite different conclusions are drawn.

Other isotope observations are compared with the Base Case model results in Table 6. The depth-integrated change in oceanic $\delta^{13}C$, the $\delta^{13}C$ penetration depth, and the variation in mixed layer $\delta^{13}C$ and $\Delta^{14}C$ as obtained by the model all lie within the observational uncertainty. Since the model parameters that are not tightly constrained by observations were obtained entirely by tuning the model to fit the pre-industrial tracer distributions, the ability of our model to closely simulate observed transient isotope changes is an independent test of the model performance. However, this ability serves as a meaningful constraint on the model parameters only to the extent that changes in model parameters alter the transient response.

Table 6. Comparison of Observed Isotopic Changes, Beyond Those Shown in Figure 6, with the Base Case Model Results

Variable	Model Value	Observed Value
Oceanic bomb ^{14}C inventory start of 1975	264 x 10^{26} atoms	305±31[a]
Oceanic bomb ^{14}C mean penetration depth, start of 1975	316 m	326[b]
Depth integrated $\Delta\delta^{13}C$, 1970-1990	-165‰m	-208±45[c]
$\delta^{13}C$ penetration depth, 1970-1990	524 m	520±115[d]
Mixed layer $\delta^{13}C$ decrease, 1800-1970	-0.45‰	-0.45±0.05[e]
Mixed layer $\delta^{13}C$ decrease, 1970-1990	-0.32‰	-0.39[f]
Mixed layer change in $\Delta^{14}C$, 1850-1950	-7.2‰	-9±3[g]

[a] *Broecker et al.* [1995].
[b] This is the reanalysis *of Broecker et al.*'s [1995] data by *Jain et al.* [1995].
[c] *Quay et al.* [1992].
[d] *Quay et al.* [1992].
[e] Based on changes in Bermuda coral [*Nozaki et al.*, 1978; *Druffel and Suess*, 1983].
[f] Global estimate of *Quay et al.* [1992].
[g] Radiocarbon measurements for Pacific and Atlantic corals [*Druffel and Linick*, 1978; *Druffel and Suess*, 1983].

5.2. Sensitivity of the Transient Isotope Response

The mixing parameters that could potentially exert an important influence on the transient isotopic response are the air-sea exchange coefficient (K_{as}), the background diffusion coefficient (K_n) and upwelling velocity (w), and the supplemental diffusion coefficient ($K_1(0)$). We therefore ran a series of transient response experiments in which these parameters were varied in the same way as for the spin-up results shown in Figure 6, thereby allowing us to determine the extent to which failure to correctly simulate the spin-up isotope (and other) profiles matters for the simulation of transient isotopic variations.

Figure 7 shows the effect of varying $K_1(0)$ for DIC from 0.0 $cm^2\ s^{-1}$ to 3.5 $cm^2\ s^{-1}$ (twice the Base Case value) on the transient variation of atmospheric $\delta^{13}C$ and $\Delta^{14}C$, the vertical profile of bomb ^{14}C, and the global mean penetration depth and oceanic inventory of bomb ^{14}C. Variation in the value of $K_1(0)$ has a dramatic effect on the transient isotope simulation, just as it does on the spin-up profiles (Figures 6a and 7a). The largest effects are on the vertical profile of bomb ^{14}C, on the mean penetration depth, and on the oceanic ^{14}C inventory. Varying $K_1(0)$ from half to twice the Base Case value causes the atmospheric $\delta^{13}C$ change between 1975-1990 to differ by 0.15% and the Suess effect from 1765-1950 to differ by 2.7%. The uncertainty in the estimated observed change in $\Delta^{14}C$ cited above (±1.2‰) is substantially smaller, but the scatter in the unsmoothed at-

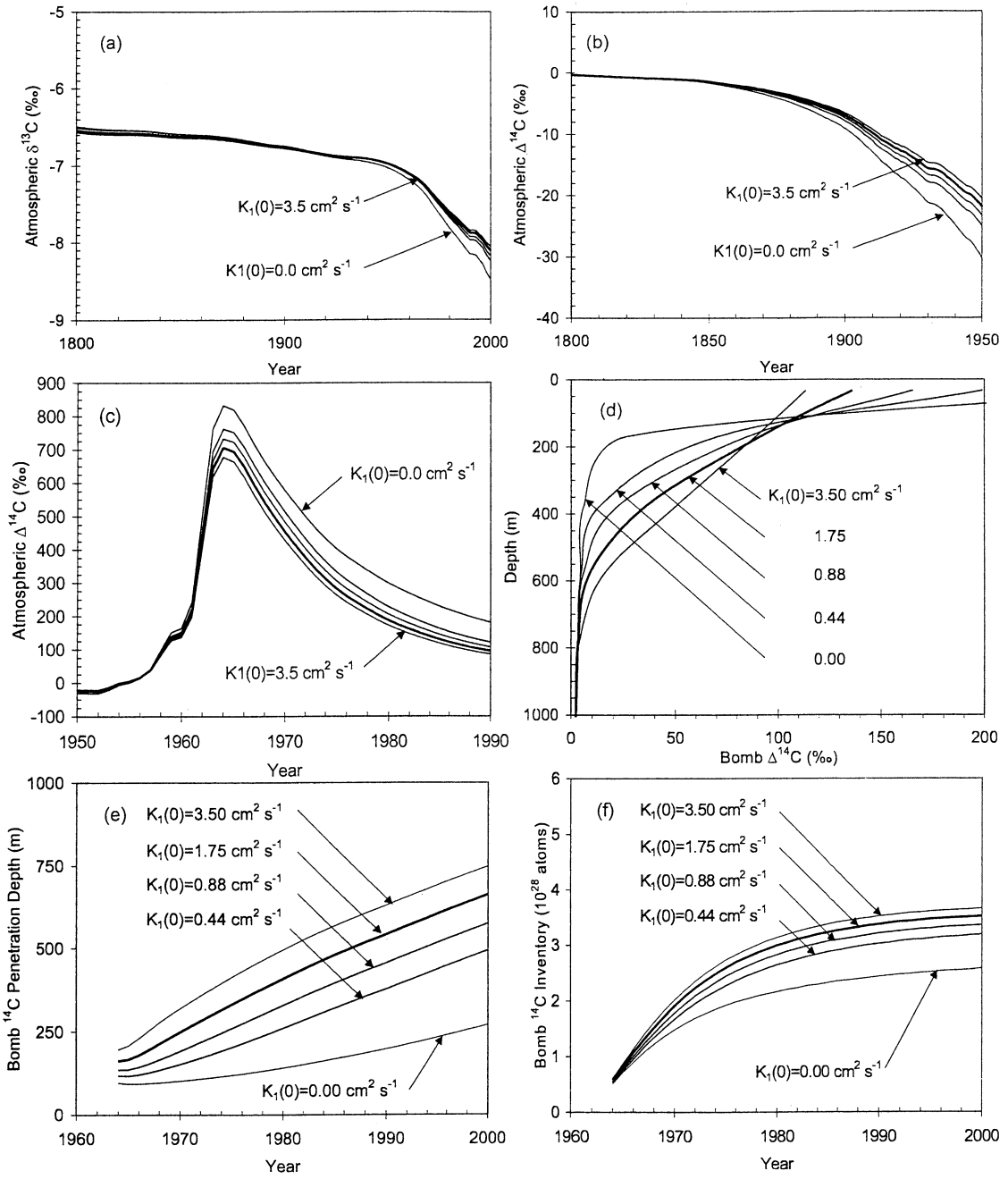

Figure 7. Impact of changes in the value of the supplemental diffusion coefficient at the base of the mixed layer, $K_1(0)$, on (a) the variation of atmospheric $\delta^{13}C$, (b) the variation of atmospheric $\Delta^{14}C$ prior to the period of nuclear bomb testing; (c) the variation of tropospheric $\Delta^{14}C$ from 1950-1990; (d) the global mean profile of bomb ^{14}C on January 1st, 1975, (e) the bomb ^{14}C penetration depth, and (f) the bomb ^{14}C inventory.

mospheric $\delta^{13}C$ measurements suggests an uncertainty in the observed $\delta^{13}C$ change comparable to the effect of varying $K_1(0)$.

Figure 8 shows the effect of doubling the nonpolar K_{as} and the upwelling and downwelling polar K_{as} on the transient variation of atmospheric $\delta^{13}C$ and $\Delta^{14}C$, and on the vertical profile of bomb ^{14}C. These changes have a negligible effect on the $\delta^{13}C$ trend (unlike changes in $K_1(0)$) but have a much larger effect on the preindustrial $\delta^{13}C$ value than changing $K_1(0)$. Changes in the atmospheric $\Delta^{14}C$ variation are smaller than the effect of changing $K_1(0)$ by a factor of 2 but are larger than the observational uncertainty (at least after 1965, where the uncertainty is essentially zero). The effect of changing K_{as} on the ocean bomb $\Delta^{14}C$ profile (Figure 8d) is qualitatively different from the effect changing $K_1(0)$ since, in the latter case, $\Delta^{14}C$ values shift in different directions above and below a depth of 150 m but move in the same direction at all depths when K_{as} is altered.

In contrast to changes in $K_1(0)$ and K_{as}, varying K_n and w by a factor of 2 alters the trends in atmospheric $\delta^{13}C$ and $\Delta^{14}C$ or in oceanic bomb ^{14}C by no more than a few percent. This can be explained by the fact that K_n makes a very small contribution to the total K in the upper ocean and by the fact that advection is much less important to the mixed layer carbon budget than is diffusion.

To conclude this section, the only model parameters that are

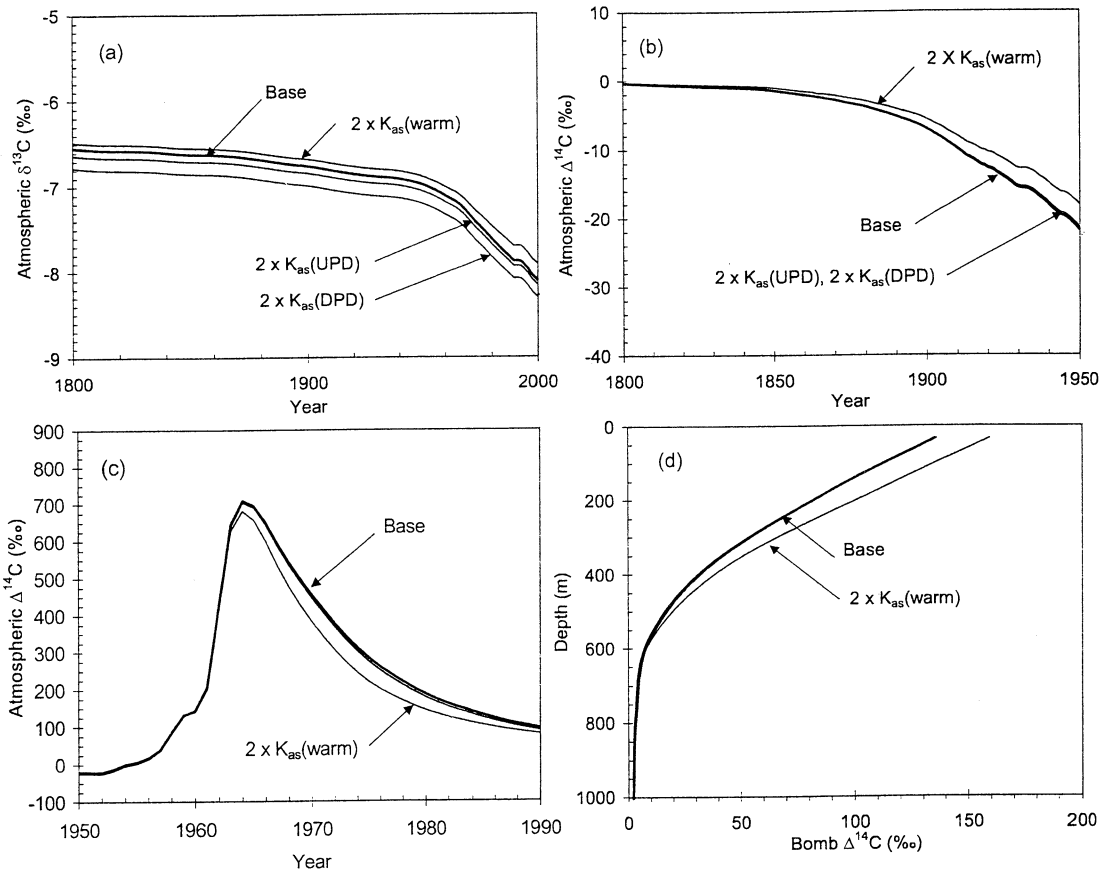

Figure 8. Impact of changes in the air-sea exchange coefficient, K_{as}, on (a) the variation of atmospheric δ^{13}C, (b) the variation of atmospheric Δ^{14}C prior to the period of nuclear bomb testing; (c) the variation of tropospheric Δ^{14}C from 1950-1990; and (d) the global mean profile of bomb ^{14}C on January 1, 1975.

important to the transient isotopic variations are $K_1(0)$ and K_{as}. Alteration of these parameters from the values obtained by tuning them to the preindustrial tracer distributions noticeably degrades the transient simulation compared to the uncertainties in the observations. The successful simulation of transient isotope variations therefore serves as an independent validation of the model parameters.

5.3. Impact on Atmospheric CO_2 Variation

In order to illustrate the impact of changes in the model parameters on the concentration of atmospheric CO_2, we ran the model using the Intergovernmental Panel on Climate Change (IPCC) IS92a fossil fuel emission scenario [*Leggett et al.*, 1992], in which emissions increase to 20.4 Gt C yr^{-1} by 2100. This scenario was extended to the year 2200 by assuming that emissions decrease by 1% per year after 2100. Figure 9 shows the atmospheric CO_2 concentration as $K_1(0)$, K_n, and w are varied. Varying $K_1(0)$ from half to twice the Base Case value has a remarkably small effect on future atmospheric CO_2, with the concentration in 2200 ranging from 1073 to 1159 ppmv as $K_1(0)$ varies by a factor of 4. A somewhat smaller range occurs as K_n and w are doubled. Figure 10 shows the corresponding variation in the rate of oceanic CO_2 uptake. The oceanic uptake averaged over 1980-1990 is 1.84 Gt C yr^{-1} for the Base case, which falls within the range of 2.0±0.6 Gt C yr^{-1} given by *Siegenthaler and Sarmiento* [1993]. This drops to 1.14 Gt C yr^{-1} for $K_1(0)$=0.0 cm^2 s^{-1} and increases to 2.01 Gt C yr^{-1} if $K_1(0)$ is doubled. Doubling $K_1(0)$ increases the cumulative uptake to 1990 by ~14%, whereas doubling the polar K_{as} increases the cumulative oceanic CO_2 uptake by only 2% in spite of the fact that the polar region is responsible for 15% of the cumulative oceanic uptake to 1990 and that deep mixing occurs.

Harvey and Schneider [1985] and part 1 noted that doubling K_n and w have opposing effects on the transient surface temperature response to a given radiative forcing in the classical UD model; a larger K_n gives a slower response because the thermal perturbation diffuses more strongly into the deeper ocean, whereas a larger w gives a faster response because the downward diffusing heat is more strongly advected back up into the mixed layer in the nonpolar domain. It was shown in part 1 that the transient temperature response of the Q1D model is very slightly slower when w is doubled, implying slightly faster uptake of heat by the ocean. The slightly greater uptake of carbon when w is doubled is consistent in sign with the effect of a doubled upwelling on the transient temperature response.

On the basis of these results, it can be concluded that (1) either the spin-up profiles or the transient isotope response can be used to constrain $K_1(0)$ and K_{as}; (2) the transient isotopic responses cannot be used to set a strong constraint on K_n or w because of the low sensitivity of the transient response to these variables (fortunately, however, the spin-up profiles can be used to constrain both the overall magnitude and the shape of the vertical variation of K_n and w); and (3) the oceanic uptake of anthropogenic CO_2 and future atmospheric CO_2 concentrations display essentially no sensitivity to K_{as} (in spite of the presence of a well-mixed polar sea) and only very weak sensitivity to $K_1(0)$, K_n, and w.

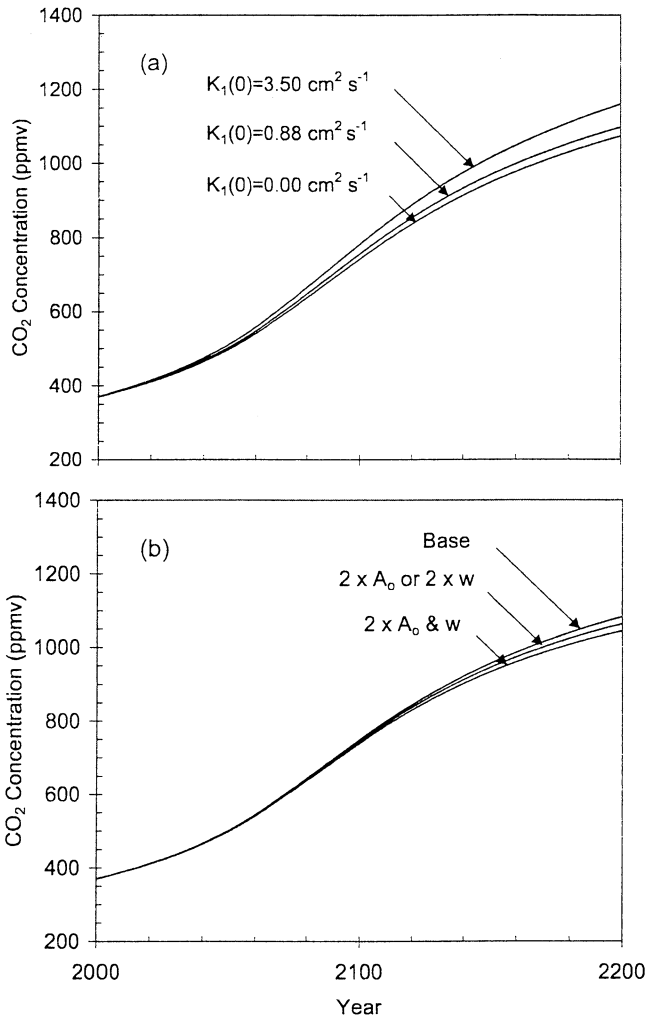

Figure 9. Impact of (a) changes in the value of the supplemental diffusion coefficient at the base of the mixed layer, $K_1(0)$, or (b) a doubling of K_n and/or w on atmospheric CO_2 concentration (ppmv).

6. Sensitivity of Atmospheric pCO_2 to the Nonpolar Ocean Surface Temperature

An important property of carbon cycle models is the sensitivity of atmospheric pCO_2 to changes in the temperature of the nonpolar ocean surface. *Broecker et al.* [1999] compared this sensitivity across a wide range of carbon cycle models: box models, a two-dimensional (2-D) model, and 3-D models. They quantify the pCO_2 sensitivity through what they call the "Harvardton Bear Equilibration Index" (HBEI), which can be defined as

$$\mathrm{HBEI} = \frac{(\Delta pCO_2)_{eq}}{(\Delta pCO_2)_o}, \qquad (2)$$

where $(\Delta pCO_2)_o$ is the change in pCO_2 of the warm surface water (defined as the region from 40°S to 40°N) the instant the temperature of the warm mixed layer has changed, and $(\Delta pCO_2)_o$ is the change in pCO_2 after equilibrium between the atmosphere and mixed layer has been reestablished. For two OGCMs, HBEI=0.243 and 0.32, whereas box models give values ranging from 0.11 to 0.28 and the 2-D ocean model of *Marchal et al.* [1998] gives an HBEI of 0.14. Since the warm ocean surface for these calculations occupies 0.66 of the ocean surface area, the size of the nonpolar domain in the present model was reduced to the same surface area (it originally having been 0.9 of the ocean surface area), and the HBEI calculated. The result obtained here is 0.28, equal to the average of the two OGCMs, and substantially more than most other non-OGCM models. This serves as another validation of the present model.

7. Concluding Comments

This paper and the accompanying part 1 have presented what is essentially a 1-D coupled climate-carbon cycle model, the only departure from its 1-D nature arising from the fact that we resolve two separate polar sea regions. In one of the polar regions, bottom water is conditioned by interaction with the atmosphere, lateral exchanges, and convective mixing, and is then injected into the deep ocean. In the other polar region, upwelling water enters from intermediate depths. This model differs in several ways from previously developed 1-D and quasi-one-dimensional models: in the model structure, in the simulation of a wider ranger of tracer fields (thereby providing further observational constraints and potential feedbacks), in the treatment of convective mixing and air-sea exchange in the polar regions, in the formulation of the vertical diffusion coefficient, and in the vertical structure of the vertical diffusion coefficient and upwelling velocity.

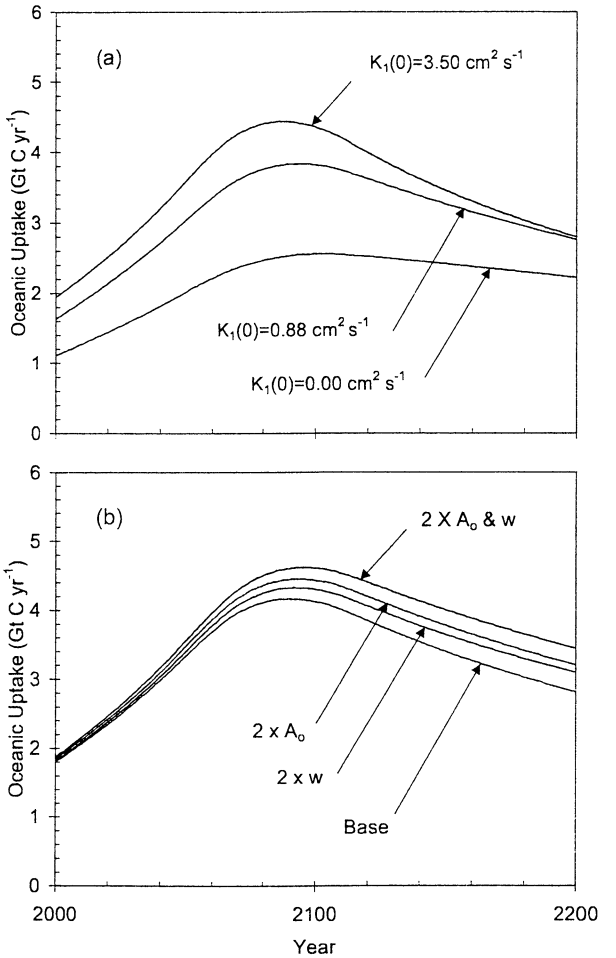

Figure 10. Same as Figure 9, except for the oceanic uptake of carbon.

Tuning the model to fit observed (or estimated) preindustrial oceanic tracer profiles and other observations requires a peak upwelling velocity of the order of 2 m yr^{-1}, a vertical diffusion coefficient (K) for carbon that is an order of magnitude larger than for temperature at the mixed layer base but which merges with the K for temperature at a depth of 500 m, and then a marked increase in K in the deep ocean. As shown in part 1, this variation in K follows naturally from physical considerations. A significant alteration in any of the Base Case parameter values significantly degrades the spin-up simulation, and no other combination of parameters could be found which does as well in simultaneously simulating so many tracer fields. Furthermore, the Base Case parameter values give an almost perfect fit of the model transient isotope variations (due to the burning of fossil fuels and nuclear bomb testing) to observed isotope variations. Alteration of $K_1(0)$ or K_{as} by a factor of 2 significantly degrades this performance as well.

The inclusion of alkalinity, which has been generally neglected in previous 1-D models, moderates the response of mixed layer pCO_2 to changes in model parameters, and affects the vertical carbon transfer associated with thermohaline overturning. The latter arises because relatively high surface alkalinity in polar regions allows a larger dissolved inorganic carbon content of sinking water than would otherwise be the case. The net alkalinity flow due to biological activity is downward in the nonpolar domain and upward in the polar domains, so uniform changes in biological productivity will have opposing effects on surface alkalinity (and hence surface pCO_2) in polar and nonpolar regions.

In contrast to the high sensitivity of the model spin-up state and transient isotope variations to changes in the model parameters, the simulated variation of atmospheric CO_2 concentration to the year 2200 is remarkably insensitive to rather large changes in the model parameters. This suggests that the choice of model parameters (and the details of the model formulation, such as the difference between the present model and that of *Jain et al.* [1995]) is not important for the simulation of future atmospheric CO_2 concentrations. This conclusion is probably justified for "surprise-free" scenarios, in which ocean circulation changes do not occur. However, if large ocean circulation changes occur as part of the transient response (which would be represented in the present model by a change in the peak w or its vertical profile), this could have a larger effect on simulated future CO_2 simulations than the choice of different, but fixed, values of w and other parameters.

Although the ability to simulate past isotope variations tells us nothing about the likelihood of future ocean circulation changes, it could very well provide some constraints on the impact of such changes on atmospheric CO_2. This is because the effect of ocean circulation changes on atmospheric CO_2 could very well depend on the absolute magnitudes and relative importance of the various carbon, alkalinity, and phosphorous fluxes between the mixed layer and the deep ocean, and the interaction between these fluxes. These in turn depend on the choice of model parameters, which are constrained by the spin-up and transient isotope observations. These important issues are explored elsewhere (L.D.D. Harvey, manuscript in preparation, 2001). Furthermore, the choice of mixing parameters and the spin-up model state (even for versions which give the same preindustrial atmospheric pCO_2) could very well be important to the simulation of past atmospheric CO_2 changes and in possible internal oscillations involving temperature changes and the carbon cycle. The fact that the sensitivity of the model atmospheric pCO_2 to changes in the temperature of warm ocean surface temperatures matches that obtained by 3-D ocean carbon cycle models, lends further support to the use of the present model in investigating climate-carbon cycle interactions.

Finally, the present model dispenses with the unjustified assumption that the effective vertical diffusion coefficients for heat and for carbon (and other tracers) need be the same. In purely climate upwelling diffusion models, only the ratio of K_v to w (the upwelling velocity) can be constrained from the observed temperature profile. Here, w is constrained in part from carbon data. This in turns constrains the value of K_v that will fit the observed temperature profile. The required K_v (0.15 cm^2 s^{-1} at the base of the mixed layer) is consistent with direct measurements and much smaller than required for carbon, or than has been previously used for simulating the transient temperature response to radiative heating with 1-D models (where values of 0.6-1.0 cm^2 s^{-1} are typical). The low K_v and w deduced here have implications for the empirical determination of climate sensitivity by compared observed and model-simulated temperature changes during the past 120 years. In particular, small K_v and w permit a smaller climate sensitivity than the more traditional, larger values.

Appendix A: Ocean Biological Processes

Soft tissue production in the mixed layer during a time step, P_{soft}, is computed as

$$P_{soft} = L_{fac} P_{fac} R_{CP} [PO_4^{3-}] \quad , \tag{A1}$$

where L_{fac} accounts for differences between polar and nonpolar domains in the availability of light during the growing season, P_{fac} is a Michaelis-Menton TPO_4 factor, R_{CP} is the carbon to phosphorus Redfield ratio, and $[PO_4^{3-}]$ is the dissolved phosphate concentration at the start of the time step. In the limiting case where $L=P_{fac}=1.0$, all of the TPO_4 in the mixed layer at the start of a given time step is consumed during the time step. The Michaelis-Menton factor is given by

$$P_{fac} = \frac{[PO_4^{3-}]}{[PO_4^{3-}] + P_h} \quad , \tag{A2}$$

where P_h is the TPO_4 concentration at which the Michaelis-Menton factor equals 0.5. All of P_{soft} produces a rain of falling particulate organic matter (POC), a small fraction of which is buried in sediment within the mixed layer while the rest is exported to the ocean below the mixed layer.

The production of $CaCO_3$ skeletal material, P_{hard}, is computed as by *Maier-Reimer* [1993], namely

$$Phard = \frac{\Phi_{CO3}^2}{\Phi_{CO3} + \Phi_{SiO2}} \tag{A3}$$

$$\Phi_{SiO_2} = \mathrm{Min}([SiO_2], S_{fac} P_{soft}) \tag{A4}$$

$$S_{fac} = \frac{[SiO_2]}{[SiO_2] + S_{half}} \tag{A5}$$

$$\Phi_{CO_3} = \frac{e^{(T-283.15)/10}}{1 + e^{(T-283.15)/10}} Pf_{CO_3} P_{soft} \cdot \tag{A6}$$

Since $[SiO_2]$ is not a model-predicted variable, we set $[SiO_2]=1$ μmole kg^{-1} in the nonpolar mixed layer and 3 μmole kg^{-1} in the polar mixed layer for the purpose of computing P_{hard}, and set $S_h=$ 4 μmole kg^{-1} (as by *Maier-Reimer*, [1993]). The factor Pf_{CO3} is a

tunable parameter that provides some control over the P_{hard}:P_{soft} ratio. The result of equations (A3) through (A6) is that significant $CaCO_3$ production occurs only in the nonpolar domain. A fraction f_{arog} of P_{hard} is assigned to arogonite production, with the remainder going to calcite. P_{hard} leads to a rain of falling $CaCO_3$ particles.

The vertical distribution of falling POC is computed by assuming that a fraction is resistant to decomposition and falls to the local ocean bottom, while the remaining flux decreases exponentially with depth using a depth scale z_{POC}. The convergence of the falling POC flux is added to the POC pool for that layer, which then decomposes with a time constant τ_{POC}. This procedure is the same as that used by *Heinze et al.* [1991], except that an exponential decay in the flux of the nonresistant POC is used here for the sake of simplicity. We obtained a value for z_{POC} of 400 m by requiring the model to match the observed depth of the subsurface oxygen minimum and TPO_4 maximum. The calcite flux is assumed to fall without dissolution en route, since *Keir* [1982] indicates that most calcite leaving the mixed layer reaches the ocean bottom intact. The arogonite flux at a given point is assumed to decrease by 0.014% per m below the arogonite saturation horizon, based on data given by *Bryne et al.* [1984].

All three fluxes are attenuated through partial deposition within each model layer, since a portion of the ocean bottom is assumed to occur within each model layer and will intercept some of the falling debris. A portion of the gross POC burial is assumed to redissolve within the bottom sediments; the fraction that redissolves is assumed to increase linearly from 0.5 at a bottom depth of 0 m, to 0.95 at a bottom depth of 6000 m, based on sedimentation flux and remineralization data presented by *Middleburg et al.* [1997]. The POC that does not dissolve leads to net burial. For calcite and arogonite, the fraction of gross burial assumed to redissolve increases with depth D below the lysocline according to

$$f_{dis} = 1 - \tanh(0.55D/1000), \qquad \text{(A7)}$$

where D is in meters. The shape of the fractional dissolution curve given by equation (A15) using D = 500-1000 m is similar to the curves shown in *Keir* [1982], in which 50% of the gross burial dissolves at a depth of ~0.5-1 km below the lysocline. The lysocline is defined as the depth at which sediment dissolution first occurs and is up to 1 km above the depth at which the carbonate saturation level occurs in the ambient water [*Emerson and Bender*, 1981]. Here we compute the lysocline for arogonite and calcite as the depth at which the CO_3^{2-} concentration times a factor Sf_{CO3} equals the saturation value, C_{sat}. The factor Sf_{CO3} accounts for the fact that decay of organic matter within ocean sediments releases CO_2 which drives down $[CO_3^{2-}]$ in the sediments, such that dissolution occurs where the ambient water is still slightly saturated. Choosing Sf_{CO3}=0.93 gives the observed offset under 1 km. For calcite, C_{sat} is given by

$$C_{sat} = 47.5 e^{-\frac{z}{6250}} \mu\text{mole/kg}, \qquad \text{(A8)}$$

(where z is in meters), as given by *Broecker and Takahashi* [1978], while C_{sat} for arogonite is equal to 1.48 that for calcite [*Feely et al.*, 1984]. The CO_3^{2-} concentration is computed using the algorithm given in the appendix to *Peng et al.* [1987].

Biological production leads to an adjustment of mixed layer DIC, TPO4, and alkalinity, the later given by

$$\Delta\text{ALK} = \left(\frac{R_{NP}+3}{R_{CP}}\right) P_{soft} - 2P_{hard}, \qquad \text{(A9)}$$

where R_{NP} and R_{CP} are the nitrogen-to-phosphorous and carbon-to-phosphorous Redfield ratios. The reverse changes occur when decay of POC occurs and, as well, decay of organic matter consumes O_2. We assume Redfield ratios C:N:P:O_2 for synthesis and decay of organic matter of 117:16:1:170, as by *Anderson and Sarmiento* [1994].

Since we assume the carbon cycle to be balanced at geological timescales, the loss of DIC and TPO_4 and the increase of TALK associated with burial of POC is assumed to be exactly offset by riverine fluxes of DIC, TPO_4 and negative TALK to the mixed layer during the model spin-up. Similarly, the burial of $CaCO_3$ is assumed to be balanced by a volcanic source of CO_2 to the atmosphere and a riverine source of TALK to the mixed layer during the model spin-up.

Finally, carbon isotope fractionation is allowed to occur during the construction of soft tissues. The fractionation factor f_m^{13} for ^{13}C is assumed to vary linearly from 0.970 at 273 K to 0.981 at 300 K, where the limits are based on *Lynch-Steiglitz et al.* [1995]. The fractionation factor for ^{14}C is given by $(f_m^{13})^2$. No fractionation is assumed during $CaCO_3$ construction or during the decay of soft tissue.

Appendix B: Air-Sea Exchange of CO_2, ^{14}C Production, and Isotope Standards

The air-to-sea flux of carbon isotope i is computed as

$$F_{as}^i = K_{as}(\alpha_{as}^i r_a^i P_a - \alpha_{sa}^i r_s^i P_s), \qquad \text{(B1)}$$

where K_{as} is the gas exchange coefficient (mole m^{-2} yr^{-1} μatm^{-1}); α_{as}^i and α_{sa}^i are kinetic fractionation factors for isotope i; r_a^i and r_s^i are the ratios of isotope i to total carbon in the atmosphere and mixed layer; and P_a and P_s are the atmospheric and mixed layer CO_2 partial pressures. The kinetic fractionation factors for ^{13}C are given by

$$\alpha_{as} = \left(1.00019 - \frac{0.373}{T}\right) 0.9995, \qquad \text{(B2a)}$$

and

$$\alpha_{sa} = \left(1.02387 - \frac{9.779}{T}\right) 0.9995, \qquad \text{(B2b)}$$

respectively, based on *Heimann and Monfray* [1989, appendix D] and *Wanninkhof* [1985]. *Yamanaka and Tajika* [1996, appendix] provide a clear physiochemical explanation of this parameterization. The kinetic fractionation factors for ^{14}C are the squares of those for ^{13}C. The CO_2 partial pressure of sea water, P_s, is computed using the algorithm given in the appendix to *Peng et al.* [1987], while the atmospheric CO_2 partial pressure is given by the atmospheric CO_2 carbon content times a fixed factor of 0.469 μatm Gt^{-1}.

Model $\Delta^{14}C$ values are computed from $\delta^{14}C$ and $\delta^{13}C$ values as by *Stuiver and Pollach* [1977], using a standard ^{13}C:C ratio of 0.0111123 and a standard ^{14}C:C ratio of 1.176 x 10^{-12}. Once the model spin-up for preindustrial conditions is achieved, the ^{14}C production rate due to cosmic rays is adjusted so that the atmospheric $\Delta^{14}C$ is exactly zero. The model ^{14}C amounts are multiplied by the same factor by which the original ^{14}C production rate was implicitly multiplied, so that the ^{14}C distribution remains in a steady state. The volcanic and riverine

sources of DIC are assumed to contain no ^{14}C, since these represent very old carbon that is recycled on a multimillion year timescale.

Appendix C: Solution Algorithm

The solution algorithm used for temperature, as described in part 1, is applied to all other tracers. In the case of temperature, the energy balance equations (equations A8 and A9 of part 1) were linearized and solved analytically. The analytical solution gives the changes in atmospheric and mixed layer temperature due to heat exchange between the atmosphere and mixed layer and due to the absorption of solar radiation. The change in atmospheric and mixed layer CO_2 content is also determined by analytically integrating the linearized equations for air-sea exchange. In this case, the linearized equations are

$$\frac{d\Delta C_a^i}{dt} = S_{CR}^i + F_T^i + F_V^i - K_{as}[\alpha_{as}^i \gamma_a (C_{ao}^i + \Delta C_a^i) - \alpha_{sa}^i \gamma_s (C_{so}^i + \beta \Delta C_s^i)] - \frac{(C_{ao}^i + \Delta C_a^i)}{\tau_i} \quad \text{(C1)}$$

$$\frac{d\Delta C_s^i}{dt} = F_D^i + F_R^i + F_M^i + K_{as}[\alpha_{as}^i \gamma_a (C_{ao}^i + \Delta C_a^i) - \alpha_{sa}^i \gamma_s (C_{so}^i + \beta \Delta C_s^i)] - \frac{(C_{so}^i + \Delta C_s^i)}{\tau_i}, \quad \text{(C2)}$$

where Caoi and Csoi are the atmospheric and mixed layer carbon amounts (Gt) at the beginning of the time step for isotope i, ΔC_a^i and ΔC_s^i are the corresponding changes during the time step, γ_a=0.469 is a factor to convert C_{ao}^i and ΔC_a^i to P_a^i and ΔP_a^i (P_a^i is the atmospheric CO_2 partial pressure for isotope i), γ_s converts from C_{so} and ΔC_s^i to P_s^i and ΔP_s^i but depends on C_{so} and the chosen mixed layer depth and is updated on each time step (P_s^i is the mixed layer CO_2 partial pressure for isotope i), $\beta = (\Delta pCO_2/pCO_2)/(\Delta DIC/DIC)$ is the buffer factor and is updated whenever DIC has changed by 0.1% since the last update, F_T^i and F_V^i are the mean annual fluxes of isotope i to the atmosphere from the terrestrial biosphere and from volcanoes (where F_T^i can be negative), F_R^i and F_M^i are the riverine and marine biosphere fluxes to the mixed layer ($F_V^i = F_R^i = 0$ for ^{14}C, and $F_M^i < 0$), F_D^i is the mean annual flux of isotope i to the mixed layer due to advection and vertical diffusion (nonpolar domain) or convection (polar domain), S_{CR}^i is the production rate due to cosmic rays (this term is present only when solving for ^{14}C), and τ_i is the time constant for radioactive decay ($\tau_i = \infty$ for ^{12}C and ^{13}C).

Acknowledgment. This research was supported by NSERC grant OGP0001413.

References

Anderson, L.A., and J.L. Sarmiento, Redfield ratios of remineralization determined by nutrient data analysis, *Global Biogeochem. Cycles*, *8*, 65-80, 1994.

Andres, R.J., G. Marland, and S. Bischof, The carbon dioxide emissions from fossil fuel combustion and cement manufacture 1751-1991 and an estimate of their isotopic composition and latitudinal distribution, in *The Carbon Cycle*, edited by T.M.L. Wigely and D.S. Schimel, pp.53-62, Cambridge Univ. Press, New York, 2000.

Bacastow, R., and E. Maier-Reimer, Ocean circulation model of the carbon cycle, *Clim. Dyn.*, *4*, 95-125, 1990.

Broecker, W.S., and T.-H. Peng, *Tracers in the Sea*, 690 pp., Lamont-Doherty Earth Observatory, Palisades, N.Y., 1982.

Broecker, W.S., and T.-H. Peng, Stratospheric contribution to the global bomb radiocarbon inventory: Model versus observation, *Global Biogeochem.Cycles*, 8, 377-384, 1994.

Broecker, W.S. and T. Takahashi, The relationship between lysocline depth and in situ carbonate ion concentration, *Deep Sea Res., 25*, 65-95, 1978.

Broecker, W.S., T.-H Peng, G. Ostlund and M. Stuiver, The distribution of bomb radiocarbon in the ocean, *J. Geophys. Res., 90*, 6953-6970, 1985.

Broecker, W.S., S. Sutherland, W. Smethie, T.-H. Peng, and G. Ostlund, Oceanic radiocarbon: Separation of the natural and bomb components, *Global Biogeochem. Cycles*, *9*, 263-288, 1995.

Broecker, W.S., J. Lynch-Stieglitz, D. Archer, M. Hofmann, E. Maier-Reimer, O. Marchal, T. Stocker, and N. Gruber, How strong is the Harvardton-Bear constraint?, *Global Biogeochem. Cycles*, *13*, 817-820, 1999.

Byrne, R.H., J.G. Acker, P.R. Betzer, R.A. Feely, and M.H. Cates, Water column dissolution of arogonite in the Pacific Ocean, *Nature*, *312*, 321-326, 1984.

Druffel, E.M., and T.W. Linick, Radiocarbon in annual coral rings of Florida, *Geophys. Res. Lett., 5*, 913-916, 1978.

Druffel, E.M., and H.E. Suess, On the radiocarbon record in banded corals: Exchange parameters and the transport of $^{14}CO_2$ between atmosphere and surface ocean, *J. Geophys. Res., 88*, 1271-1280, 1983.

Emerson, S., and M. Bender, Carbon fluxes at the sediment-water interface of the deep-sea: Calcium carbonate preservation, *J. Mar. Res.*, *39*, 139-162, 1981.

Emerson, S., P. Quay, D. Karl, C. Winn, L. Tupas, and M. Landry, Experimental determination of the organic carbon flux from open-ocean surface waters, *Nature*, *389*, 951-954, 1997.

Feely, R.A., R.H. Bryne, P.R. Betzer, J.F. Gendron, J.G. and Acker, Factors influencing the degree of saturation of the surface and intermediate waters of the North Pacific with respect to aragonite, *J. Geophys. Res.*, *89*, 10,631-10,640, 1984.

Harvey, L.D.D., Effect of model structure on the response of terrestrial biosphere models to CO_2 and temperature increases, *Global Biogeochem. Cycles*, *3*, 137-153, 1989.

Harvey, L.D.D., Transient temperature and sea level response of a two-dimensional ocean-climate model to greenhouse gas increases, *J. Geophys. Res., 99*, 18,447-18,466, 1994.

Harvey, L.D.D., and Z. Huang, A quasi-one-dimensional coupled climate-carbon cycle model, 1, Description and behavior of the climate component, *J. Geophys. Res.*, this issue.

Harvey, L.D.D., and S.H. Schneider, Transient climatic response to external forcing on 10^0-10^4 year time scales, 1, Experiments with globally averaged coupled atmosphere and ocean energy balance models, *J. Geophys. Res., 90*, 2191-2205, 1985.

Harvey, L.D.D., J. Gregory, M. Hoffert, A. Jain, M. Lal, R. Leemans, S. Raper, T. Wigley, and J. de Wolde, *An Introduction to Simple Climate Models Used in the IPCC Second Assessment Report, Tech. Pap. 2,* 53 pp., Intergovernmental Panel on Climate Change, Geneva, 1997.

Heimann, M., and P. Monfray, Spatial and temporal variation of the gas exchange coefficient for CO_2, 1, Data analysis and global validation, *Rep. 31*, 29 pp., Max-Planck-Inst. für Meteorol., Hamburg, 1989.

Heinze, C., E. Maier-Reimer, and K. Winn, Glacial pCO_2 reduction by the world ocean: Experiments with the Hamburg carbon cycle model, *Paleoceanography*, *6*, 395-430, 1991.

Hesshaimer, V., M. Heimann, and I. Levin, Radiocarbon evidence for a smaller oceanic carbon dioxide sink than previously believed, *Nature*, *370*, 201-203, 1994.

Hoffert, M.I., A.J. Callegari, and C.T. Hsieh, The role of deep sea heat storage in the secular response to climate forcing, *J. Geophys. Res.*, *85*, 6667-6679, 1980.

Jain, A., H.S. Kheshgi, M.I. Hoffert, and D.J. Wuebbles, Distribution of radiocarbon as a test of global carbon cycle models, *Global Biogeochem. Cycles*, *9*, 153-166, 1995.

Jain, A.K., H.S. Kheshgi, and D.J. Wuebbles, A globally aggregated reconstruction of cycles of carbon and its isotopes, *Tellus, Ser. B, 48B*, 583-600, 1996.

Joos, F., G.K. Plattner, T.F. Stocker, O. Marchal, and A. Schmittner,

Global warming and marine carbon cycle feedbacks on future atmospheric CO_2, *Science*, *284*, 464-467, 1999.

Keeling, C.D. and T.P. Whorf, Atmospheric CO_2 records from sites in the SIO air sampling network, in *Trends: A Compendium of Data on Global Change*, Carbon Dioxide Info. Anal. Cent., Oak Ridge Nat. Lab., Oak Ridge, Tenn., 1998.

Keir, R.S., Dissolution of calcite in the deep sea: Theoretical prediction for the case of uniform size particles settling into a well-mixed sediment, *Am. J. Sci.*, *282*, 193-236, 1982.

Kroopnick, P.M., The distribution of ^{13}C of ΣCO_2 in the world oceans, *Deep Sea Res.*, *32*, 57-84, 1985.

Leggett, J.A., W.J. Pepper, and R.J. Swart, Emissions scenarios for the IPCC: An update, in *Climate Change 1992:The Supplementary Report to the IPCC Scientific Assesstment*, edited by J.T. Houghton, B.A. Callander, and S.K. Varney, pp. 69-95, Cambridge Univ. Press, New York, 1992.

Levitus, S., *Climatological Atlas of the World Ocean*, NOAA *Prof. Pap. 13,* 173 pp., Natl. Oceanic and Atmos. Admin., Washington, D.C., 1982.

Levitus, S., M.E. Conkright, J.L. Reid, R.G. Najjar, and A. Mantyla, Distribution of nitrate, phosphate and silicate in the world oceans, *Prog. Oceanogr.*, *31*, 245-273, 1993.

Lynch-Stieglitz, J., T.F. Stocker, W.S. Broecker, and R.G. Fairbanks, The influence of air-sea exchange on the isotopic composition of oceanic carbon: Observations and modeling, *Global Biogeochem. Cycles*, *9*, 653-665, 1995.

Maier-Reimer, E., Geochemical cycles in an ocean general circulation model: Preindustrial tracer distributions, *Global Biogeochem. Cycles*, *7*, 645-677, 1993.

Maier-Reimer, E., and K. Hasselmann, Transport and storage of CO_2 in the ocean - An inorganic ocean-circulation carbon cycle model, *Clim. Dyn.*, *2*, 63-90, 1987.

Maier-Reimer, E., U. Mikolajewicz, and A. Winguth, Future ocean uptake of CO_2: Interactions between ocean circulation and biology, *Clim. Dyn.*, *12*, 711-721, 1996.

Marchal, O., T.F. Stocker, and F. Joss, A latitude-depth, circulation-biogeochemical ocean model for paleoclimate studies. Development and sensitivities, *Tellus*, *Ser. B, 50B*, 290-316, 1998.

Marland, G., T.A. Boden, R.J. Andres, A.L. Brenkert, and C. Johnston, Global, regional, and national CO_2 emissions, in *Trends: A Compendium of Data on Global Change*, Carbon Dioxide Info. Anal. Center, Oak Ridge Nat. Lab., Oak Ridge, Tenn., 1998.

Middelburg, J.J., K. Soetaert, and P.M.J. Herman, Empirical relationships for use in global diagenetic models, *Deep Sea Res.*, *44*, 327-344, 1997.

Moum, J.N., and T.R. Osborn, Mixing in the main thermocline, *J. Phys. Oceanogr.*, *16*, 1250-1259, 1986.

Nozaki, Y., D.M. Rye, K.K. Turekian, and R.E. Dodge, A 200 year record of carbon-13 and carbon-14 variations in Bermuda coral, *Geophys. Res. Lett.*, *5*, 825-828, 1978.

Opdyke, B.N., and C.G. Walker, Return of the coral reef hypothesis: Basin to shelf partitioning of $CaCO_3$ and its effect on atmospheric CO_2, *Geology*, *20*, 733-736, 1992.

Peng, T.H., T. Takahashi,, W.S. Broecker, and J. Olafsson, Seasonal variability of carbon dioxide, nutrients and oxygen in the northern North Atlantic surface water: Observations and a model, *Tellus*, *Ser. B, 39B*, 439-458, 1987.

Quay, P.D., B. Tilbrook, and C.S. Wong, Oceanic uptake of fossil fuel CO_2: Carbon-13 evidence, *Science*, *256*, 74-79, 1992.

Sarmiento, J.L. and C. Le Quéré, Oceanic carbon dioxide uptake in a model of century-scale global warming, *Science*, *274*, 1346-1350, 1996.

Sarmiento, J.L., J.C. Orr, and U. Siegenthaler, A perturbation simulation of CO_2 uptake in an ocean general circulation model, *J. Geophys. Res.*, *97*, 3621-3645, 1992.

Schimel, D., M. Brubb, F. Joos, R. Kaufmann, R. Moss, W. Ogana, R. Richesl, and T. Wigley, *Stabilization of Atmospheric Greenhouse Gases: Physical, Bioloigcal and Socio-ecnomic Implications*, *Tech. Pap. 3*, 52 pp., Intergovernmental Panel on Clim. Change, Geneva, 1997.

Shaffer, G., Biogeochemical cycling in the global ocean, 2, New production, Redfield ratios, and remineralization in the organic pump, *J. Geophys. Res.*, *101*, 3723-3745, 1996.

Shaffer, G., and J.L. Sarmiento, Biogeochemical cycling in the global ocean, 1, A new, analytical model with continuous vertical resolution and high latitude dynamics, *J. Geophys. Res.*, *100*, 2659-2672, 1995.

Siegenthaler, U., and F. Joos, Use of a simple model for studying oceanic tracer distributions and the global carbon cycle, *Tellus*, *Ser. B, 44B*, 186-207, 1992.

Siegenthaler, U., and J.L. Sarmiento, Atmospheric carbon dioxide and the ocean, *Nature*, *365*, 119-125, 1993.

Stocker, T.F., D.G. Wright, and L.A. Mysak, A zonally averaged, coupled ocean-atmosphere model for paleoclimatic studies, *J. Clim.*, 5, 773-797, 1992.

Stocker, T.F., W.S. Broecker, and D.G. Wright, Carbon uptake experiments with a zonally-averaged global ocean circulation model, *Tellus*, *Ser. B, 46B*, 103-122, 1994.

Stuiver, M. and H. Pollach, Discussion reporting of ^{14}C data, *Radiocarbon*, *19*, 355-363, 1977.

Stuiver, M., and P.D. Quay, Atmospheric ^{14}C changes resulting from fossil fuel CO_2 release and cosmic ray flux variability, *Earth Planet. Sci. Let.*, *53*, 349-362, 1981.

Sundquist, E.T., Long-term aspects of future atmospheric CO_2 and sea-level changes, in *Sea Level Change*, edited by R. Revelle, pp. 193-207, Nat. Acad. Press, Washington, D.C., 1990.

Takahashi, T., W.S. Broecker, and A.E. Bainbridge, The alkalinity and total carbon dioxide concentration in the world oceans, in *Carbon Cycle Modelling*, *SCOPE 16*, edited by B. Bolin, pp. 271-286, John Wiley, New York, 1981.

Takahashi, T., J. Olafsson, J.G. Goddard, D.W. Chipman, and S.C. Sutherland, Seasonal variation in CO_2 and nutrients in the high-latitude surface oceans: A comparative study, *Global Biogeochem. Cycles*, *7*, 843-878, 1993.

Tans, P., $^{13}C/^{12}C$ of industrial CO_2, in *Carbon Cycle Modeling, SCOPE 16*, edited by B. Bolin, pp. 127-129, John Wiley, New York, 1981.

Tans, P.P., I.Y. Fung, and T. Takahashi, Observational constraints on the global atmospheric CO_2 budget, *Science*, *247*, 1431-1438, 1990.

Taylor, N.K., Seasonal uptake of anthropogenic CO_2 in an ocean general circulation model, *Tellus*, *Ser. B*, 47B, 145-169, 1995.

Wanninkhof, R., Kinetic fractionation of the carbon isotopes ^{13}C and ^{12}C during transfer of CO_2 from air to seawater, *Tellus*, *Ser. B, 37B*, 128-135, 1985.

Wigley, T.M.L., A simple inverse carbon cycle model, *Global Biogeochem. Cycles*, *5*, 373-382, 1991.

Yamanaka, Y., and E. Tajika, The role of the vertical fluxes of particulate organic matter and calcite in the oceanic carbon cycle: Studies using an ocean biogeochemical general circulation model, *Global Biogeochem. Cycles*, *10*, 361-382, 1996.

L.D. Danny Harvey, Department of Geography, University of Toronto, 100 St. George Street, Toronto, Ontario, Canada M5S 3G3. (e-mail: harvey@geog.utoronto.ca)

(Received April 10, 2000; revised October 19, 2000; accepted March 20, 2001.)